

Aging Behavior Beyond SOH 80: An Experimental Aging Study on Commercial Lithium–Ion Batteries with Different Cathode Materials: Capacity Loss, Resistance Change and Impedance Modeling

Sebastian Ohneseit,* Marc C. Holocher, Alexis Kalk, Nils Uhlmann, Hans J. Seifert, and Carlos Ziebert*

New insights into lithium–ion battery aging behavior beyond a state of health of 80%, as well as for three different aging diagnostics and modeling methods, are obtained through this study conducted on four different cell types. Commercial cylindrical cells of type 21,700 are subjected to calendar aging and cyclic aging with different parameters in a long-term study. The impact of the aging parameters on the four different cathode materials assessed (lithium–nickel–manganese cobalt oxide (NMC), lithium–nickel–cobalt–aluminum oxide high energy (NCA-HE), lithium–nickel–cobalt–aluminum oxide high power, and lithium–iron phosphate oxide (LFP)) is examined with a portfolio of diagnostic methods: capacity test, Ohmic resistance test and the core

of this study, impedance analysis, together with sophisticated equivalent circuit modeling (ECM). It was found that the NMC cell degraded fastest under all aging conditions, the most durable was in most cases the NCA-HE cell. Only for one cyclic aging procedure, the LFP cells performs the best. The diagnostics shows that quantitative analysis of Nyquist plots is not sufficient for aging tracking and that some aging effects can only be detected by pulse discharging test. Moreover, capacity and mean Ohmic resistance deduced from electrochemical impedance spectroscopy test allow extrapolation to forecast further aging under diverse aging conditions.

1. Introduction

Lithium–ion batteries (LIB) have a growing worldwide application in transport and energy systems. The batteries power cars and buses for daily use, as well as energy storage applications from small home systems to grid stabilizing megabatteries. In most applications, the batteries are that much integrated into the system that a battery exchange or replacement is very costly or impossible. This is due to either safety reasons, to protect the batteries from external sources of abuse, which could lead to thermal runaway, or due to design issues, to include the battery powered propulsion technology in a way that makes it attractive for


customers. Therefore, a principal issue is the lifetime of those batteries, and a scientific question is to whether this lifetime can be extended and in which way different use scenarios affect the degradation rate.


In order to allow a safe use of batteries beyond their current end of life, we investigated the aging, safety, and materials behavior in a large aging study. This study compared four different cylindrical commercial cells of type 21,700, the cathode materials are: lithium–nickel–manganese cobalt oxide (NMC), lithium–nickel–cobalt–aluminum oxide high energy (NCA-HE), lithium–nickel–cobalt–aluminum oxide high power (NCA-HP), and lithium–iron phosphate oxide (LFP).

These cell chemistries have been previously investigated until a state of health (SOH) of 80, for example, in an extensive cyclic aging study on commercial type 18,650 cells with cathode materials NMC, NCA, and LFP from Preger et al.^[1] It showed a slower aging of LFP cells, with a larger scatter of the data compared to NMC and NCA cells, which aged faster, especially most NCA cells, for cyclic aging at different depth of discharge (DOD) and temperatures. It was concluded that reaching of SOH 80 occurs at a different number of cycles, depending on the aging conditions. LFP cells showed the highest cycle life for all conditions; however, the gap of performance becomes smaller when the energy throughput is compared, because of lower voltage and capacity of the LFP cells. Further trends for the aging parameters were found to be chemistry specific. For cycling at temperatures around room temperature, varying dominating degradation mechanism for LFP and NMC cells were attributed, as the rate of capacity fading

S. Ohneseit, N. Uhlmann, H. J. Seifert, C. Ziebert
Institute for Applied Materials-Applied Materials Physics (IAM-AWP)
Karlsruhe Institute of Technology (KIT)
Hermann-von-Helmholtz-Platz 1, 76344 Eggenstein-Leopoldshafen,
Germany
E-mail: sebastian.ohneseit@kit.edu
carlos.ziebert@kit.edu

M. C. Holocher, A. Kalk
Institute of Electrical Engineering (ETI)
Karlsruhe Institute of Technology (KIT)
Engelbert-Arnold-Straße 5, 76131 Karlsruhe, Germany

 Supporting information for this article is available on the WWW under <https://doi.org/10.1002/batt.202400713>

 © 2025 The Author(s). Batteries & Supercaps published by Wiley-VCH GmbH. This is an open access article under the terms of the Creative Commons Attribution License, which permits use, distribution and reproduction in any medium, provided the original work is properly cited.

behaved differently. Below an SOH of 80, there is very few data only; the current report is providing data until and below this SOH, by a long-term aging study over several years.

Abada et al.^[2] established a 3D electrothermal model for the mechanism leading to thermal runaway, and the aging influence on it was investigated. They showed that the thickening of solid electrolyte interface (SEI) associated with calendar aging, which hinders the diffusion of lithium ions, consequently delayed the degradation of the negative electrode during thermal abuse. This increased the onset temperature of exothermal behavior; however, the start of thermal runaway temperature is decreased.

Teichert et al.^[3] mentioned the advances of the usage of high nickel content cathodes with NMC and NCA chemistry of higher capacity and better cost efficiency. The nickel content of the cells studied in this study is given in Section 2.1. Even though the technology is advanced, new degradation routes are the consequence of the increased nickel content, especially because of a less stable interphase layer on the cathode toward the electrolyte. Also, this study suggests, to understand the aging behavior, the use of advanced characterization tools that are nondestructive, which is the case for the tools used within the current study.

Cyclic aging with an aging profile of a battery electric vehicle at different ambient temperature conditions and one calendar aging profile was studied by Kuntz et al.^[4] Electrochemical analysis was performed on half-cells, and the capacity and power fade were also analyzed. It was found that at the negative electrode, the most important degradation takes place in the form of SEI growing, for cycling at higher temperatures originating from conducting salt degradation. For low temperature cycling, both lithium deposition on the anode, as well as silicon particle cracking and disaggregation, was found. For calendar aging at 45 °C, solvent degradation was estimated as origin of the SEI growth. Additionally, comparing high power and high energy cells, it was pointed out that the thicker electrode coating of high energy cells leads to decreased kinetics because of the higher exposition at low temperature to deposition of lithium metal.

Preger et al.^[5] compared many different safety data of aged cells and the impact on critical temperatures of cell safety for different aging routes are discussed, as well as trends are found for different cathode materials and aging parameters. A direct link between aging parameters and capacity loss of commercial cells and subsequent safety is shown. Feng et al.^[6] explain how different aging defects, such as loss of active lithium and other, affect each critical temperature of the thermal runaway re-action of a cell. It also states that the same SOH from different aging routes results in different cell safety behavior during the abuse tests.

The abovementioned study shows in summary that the cell aging is directly linked to their safety and to understand the safety of aged cells; first, their aging needs to be studied in detail, which is the aim of our work for the mentioned cells and conditions.

Our tests showed that aged batteries have a higher heat dissipation, which can lead to thermal risks and in worst case thermal runaway. Additionally, the incorrect assessment of the SOH can either lead to an inefficient underestimation or a potentially dangerous overestimation of the battery system capabilities. A suitable method for SOH estimation is impedance spectroscopy, and different models are used to fit the obtained data. Based on Kallel et al.^[7]

we studied the relation of SOH and partial components of the polarization resistance. Consequently, the initially proposed linear approach has been modified for a more precise application.

The dissertation of Gantenbein^[8] examined the modeling of lithium-ion degradation based on capacity and impedance data. Therefore, extensive cyclic and calendar aging studies have been conducted on NCA and NMC, 18,650 cylindrical cells. Gantenbein points out the importance of evaluating partial elements of the cell impedance as these undergo different characteristic changes with progressing degradation. Moreover, this study looks at the aging behavior of parameters extracted from impedance models as well as capacity and hybrid pulse power characterization (HPPC) data.

In another dissertation by Illig,^[9] a model system for a LiFePO₄ cell was established, based on a commercial 18,650 cell, and the impedance behavior was described over a large range of frequencies, as well as the major losses were identified. It is stated that the association between electrochemical impedance spectroscopy (EIS) analysis of commercial cells with LFP cathode material and degradation processes is difficult, and both measurement and data treatment need specific parameters to be successful.

Those two dissertations represent fundamental and extensive work based on type 18,650 cells; the data of our study aims to support this work by furnishing data of type 21,700 cell to allow a comparison and scale-up of the model.

The motivation, to cover and compare different diagnostic techniques in this research, is based, for example on a publication by Wagner and Lowenstein,^[10] where the importance of diagnostics for product design and the possibility to derive risk and cost reduction is explained. It can be established by fundamental understanding of the relationship between the behavior of each component and its functioning, as well as between a failure and the underlying root cause. Another motivation comes from Shabbir et al.^[11] where an algorithm for health classification was developed, based on EIS scans with different states of health from capacity loss. Moreover, Ovejas and Cuadras^[12] studied NMC and LFP cells and found a direct relation from the increase in cycling charge overvoltage to an increase in open circuit voltage hysteresis and attributed this to the graphite anode of both cell types.

We have additionally studied the impact of an aging program with realistic cycles that is based on different real routes, which include traffic influence, inclination, recuperation, profiles with highway, and city and rural routes, and reported the electrochemical degradation of the tested LFP cell by Kalk et al.^[13]

Based on the literature, we have identified the following topics that are of further interest. They are covered in our research and the related data are provided in this article:

- 1) For long-term aging beyond a SOH 80;
- 2) For the type 21,700 cylindrical cell format;
- 3) To compare high-energy and high-power cells;
- 4) To directly compare NMC, NCA, and LFP cathode chemistry for the same aging parameters;
- 5) For diagnostic of aging by examining capacity loss and electrochemical impedance spectroscopy;
- 6) For characterization of aging with pulse discharge compared to electrochemical impedance spectroscopy;
- 7) For modeling approaches of the SOH of aged commercial cells.

2. Experimental Section

2.1. LIB Studied

In this study, we compared type 21,700 LIBs that were commercially available and that were acquired from different manufacturers. It was paid attention that all cells used in the aging tests came from the same batch and that the cells with the highest commercially available capacity were selected for each cathode chemistry for the study so that we thought that the latest and most relevant technology was used. We studied cells from the same batch for each cathode chemistry thoroughly in terms of their thermal safety and mechanical safety, by heat–wait–seek tests with accelerating rate calorimetry, as well as nail penetration tests, both at several states of charge.^[14] We also performed CT scans and chemical analysis on both active material and electrolyte and presented the findings in the same study. In total, we included 231 cells in this aging study and compared their behavior. The most important parameters of the cells for the aging, as well as the limits and capabilities of the cells given in the datasheet, are summarized in **Table 1**.

2.2. Laboratory Equipment

All cells were regularly assessed for their capacity, Ohmic resistance, and impedance before and during the aging. The test protocol is presented in Section 2.4, where the system used was a Biologic BCS 815-128 with 48 channels for simultaneous testing.

All cells cycled with Cyc1 protocol for 1 C discharge were aged in the same Digatron cyler, and all cells from Cyc2 protocol with 2 C discharge were cycled in the same Basytec cyler, to allow best comparability between different cells for the same protocol. While the cell holder in the Digatron cyler was designed so that the cells lay horizontally, in the Biologic and Basytec, the cells were vertically positioned during cycling.

All models, manufacturers and limits of the devices are given in **Table 2**.

2.3. Overview of Used Aging Protocols

In this study, we used four different aging protocols and tested calendar and cyclic aging on the same cell types and chemistries, all from one batch for each chemistry, guaranteeing a good comparability.

For cyclic aging, cell charging was done at C/2 in a CC–CV protocol; as recommended by the cell manufacturers, CV cutoff voltage was fixed on the full charge definition of each cell provided in the cell data sheet. Discharge was done at 1 C for Cyc1 profile and at 2 C for Cyc2 profile in a CC protocol. The DOD was always 100%, equaling a full discharge, as it was limited by reaching the discharge limit voltage of each cell. A waiting time of 30 min was followed by the CC discharge of either 1 or 2 C, depending on the profile. The full profile is given as an example for a NCA and a LFP cell in **Figure 1**, as those have different voltage limits.

During cycling, the temperature of the cells was monitored, and a safety temperature was fixed, where cycling was stopped. This safety temperature was for some cells (mainly NMC) the reason, why we stopped their aging, as they continuously reached it during discharge after more than two thousand cycles, when they had a significant aging below SOH 80. Further safety settings were upper and lower voltage limits that were set based on the cell datasheets for each battery. All aging protocols are summarized with the respective temperature and check-up conditions, which were based on the estimated capacity loss by the different profile, in **Table 3**.

2.4. Measurement Parameters and Characterization Profile: CRZ Test

The testing of the cells before and during the aging that was performed on the Biologic BCS-815 was always performed with the same program for each cell chemistry. This test is called CRZ test, as it assessed capacity (C), Ohmic resistance (R), and impedance (Z) in one program and allowed to track and characterize the degradation by different complementary parameters.

Table 1. Materials composition and electrochemical parameters of assessed cells.

Cell	Cathode composition	Anode composition	Mean capacity with 1/3 C charge in Ah	Maximum continuous discharge rate in C	CC charge limit voltage in V	CV charge cut-off current in mA	CC discharge limit voltage in V	CV charge cut-off current in mA	CC discharge limit voltage in V
NMC	$\text{Li}_x\text{Ni}_{0.807}\text{Mn}_{0.092}\text{Co}_{0.102}\text{O}_2$	carbon + 1.6% silicon	4959	3 ^{a)}	4.2	50	2.5	50	2.5
NCA-HE	$\text{Li}_x\text{Ni}_{0.879}\text{Co}_{0.107}\text{Al}_{0.014}\text{O}_2$	carbon + 1.4% silicon	4893	2	4.2	98	2.5	98	2.5
NCA-HP	$\text{Li}_x\text{Ni}_{0.878}\text{Co}_{0.107}\text{Al}_{0.015}\text{O}_2$	carbon + 1% silicon	3892	11 ^{b)}	4.2	50	2.5	50	2.5
LFP	LiFePO_4	Carbon no silicon	3117	3 ^{c)}	3.65	60	2.0	50	2.5

^{a)}3 C between 10 to 25 °C, 1.5 C between 25 to 55 °C. ^{b)}Maximum current of 45 A, corresponding to about 10.7 C for nominal cell capacity. ^{c)}3 C above 0.

Table 2. Overview of cycling and testing devices and their accuracy.						
Company	Model	Usage	Maximum current in A	Voltage measurement accuracy	Current measurement accuracy	Current control accuracy
Biologic	BCS 815-128	C, R, Z measurement	15	<0.3 mV \pm 0.01% of setting	<0.3% of value \pm 0.04% of 10 A	<0.3% of value \pm 0.04% of 10 A
Basytec	XCTS-25A	2 C discharge cyclers	25	2.5 mV	50 mA	50 mA
Digatron	MCT 50-06-24 ME	1 C discharge cyclers	50	\pm 0.1%	\pm 0.1%	\pm 0.1%
Binder	KB115, KB400, KT53, MK56	Incubators for all tests	–	–	–	–

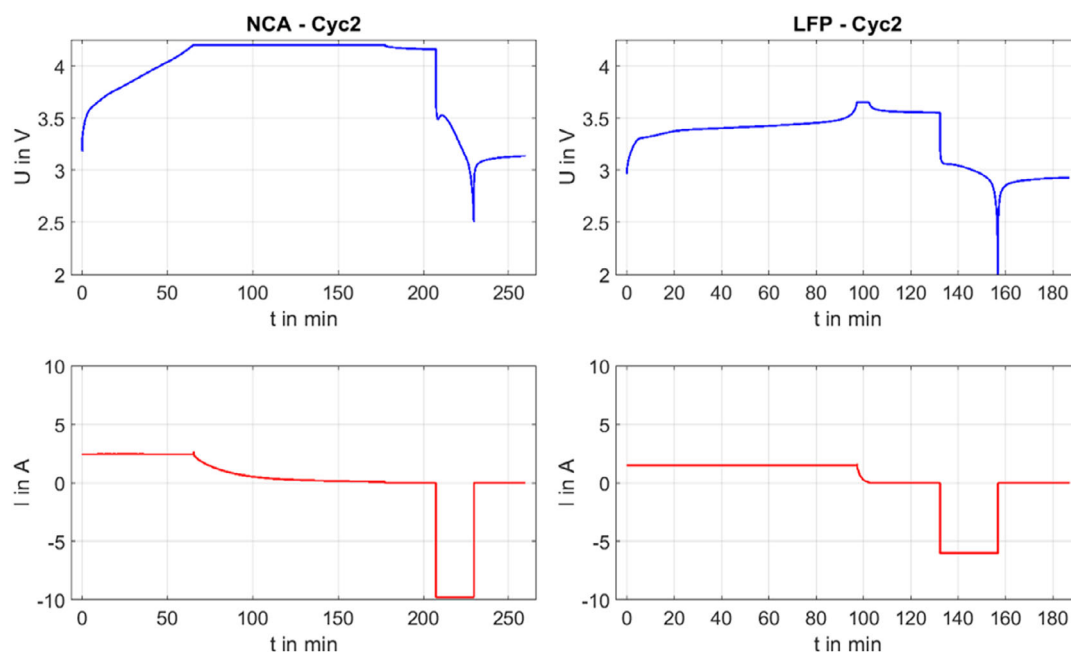


Figure 1. Example of one cycle of the cyclic aging program Cyc2 with a discharge rate of 2 C, given for an NCA-HE cell (left) and for a LFP cell (right) with voltage in blue and electric current in red colors, respectively as a function of time.

Table 3. Overview of the aging protocols, including parameters, conditions and checkup frequency.				
Program	Aging parameter	Temperature conditions [°C]	Checkup frequency	Temperature safety limit [°C]
Cyc1	0.5 C CC-CV charge 1 C discharge	20	Every 100 cycles	65
Cyc2	0.5 C CC-CV charge 2 C discharge	20	Every 50 cycles	65
Cal1	Cell stored at SOC 30	–20	Every 2 months	–
		25	Every 4 months	–
		60	Every month	–
Cal2	Cell stored at SOC 100	–20	Every 2 months	–
		25	Every 4 months	–
		60	Every month	–

For the capacity measurement, most manufacturers set the standard capacity to be obtained with a 1/3 C CC/CV charge/discharge program or a higher C rate; therefore, we fixed 1/3 C as standard CC charging and discharging rate for capacity determination and used the manufacturers current limit for the CV charging of each cell. To exclude irreversible effects from

fast charging or discharging of the batteries, the cells were fully charged and discharged twice with 1/3 C during the test, and the last 1/3 C discharge was used to obtain the capacity of the cell. At the very start of the test, another 1/3 C discharge sets the cell to SOC 0 from the storage SOC of either 30 or 100 or the end SOC of cyclic aging of 30. This setting for the cyclic aging program was

chosen, to prevent any effects of additional calendar aging at SOC 100, when the cells are stored until characterization after the cycle, for example, over the weekend. In the characterization, after the discharge, charge–discharge, and charge–discharge sequence, the test cells are CC–CV charged with a $C/2$ rate, thereby being set for the Ohmic resistance and impedance test, which was conducted at discharge and at every 10% of SOC, starting at SOC 100 and ending at SOC 0. It starts with the Z test, which is conducted in the potentiostatic electrochemical impedance spectroscopy mode of the Biologic cycler and with the parameters given in Table 4, which are inside the recommended operating and testing array of the device for EIS testing. After the Z test, a short pulse discharge with 1 C rate was performed for 10 s, that allowed us to obtain the Ohmic resistance (R). This discharge current was allowed as continuous discharge rate for all cells and therefore judged to cause no harm to the cells during testing and thus selected. This test was conducted in the galvanostatic cycling with potentiostatic limit mode of the Biologic cycler.

The R test by pulse discharging was also used to reduce the SOC partly, and another CC discharge removed the further charge so that at the next 10% SOC step, the next Z test and following R test was possible, until SOC 0 was reached. Subsequently, the cell was charged to either SOC 30 for cyclic and calendar aging, or

SOC 100 for some cells for their calendar aging with a $1/2 C$ rate and then brought back into the aging. The full test is presented for an NCA-HE cell in Figure 2.

2.5. Measurement Error and Precision

The precision of each device, as given in Section 2.2, the safety settings for voltage, current, and temperature, as well as external parameters, such as power outages, affected this aging study, which took place during a period of three years. Errors induced by these were early stopping of few cycling tests because of overheating, the faster reaching of a limiting voltage from irreversible effects especially at high C rates, without a full charging or discharging of the battery. Some samples endured a few days of waiting between cycling and testing or during cycling because of the reasons mentioned above. The cycling temperature was needed to be set to 20 °C because of overheating at higher ambient temperatures of individuals of the new NMC cells during 2 C cycling, which have their recommended operating area between 10 and 25 °C for a continuous discharge current of up to 3 C. However, a higher or faster degradation of the NMC cell was to be expected because of this fact with the Cyc2 program. Different frequency of the checkup with the CRZ test for the

Table 4. EIS testing parameters used for the cell assessment.

Parameter	Wave type	Wave Amplitude	Start frequency	End frequency	Points per decade	Tests per frequency
Unit	–	mV	kHz	Hz	–	–
Value	Sinus	10	10	0.01	10	1

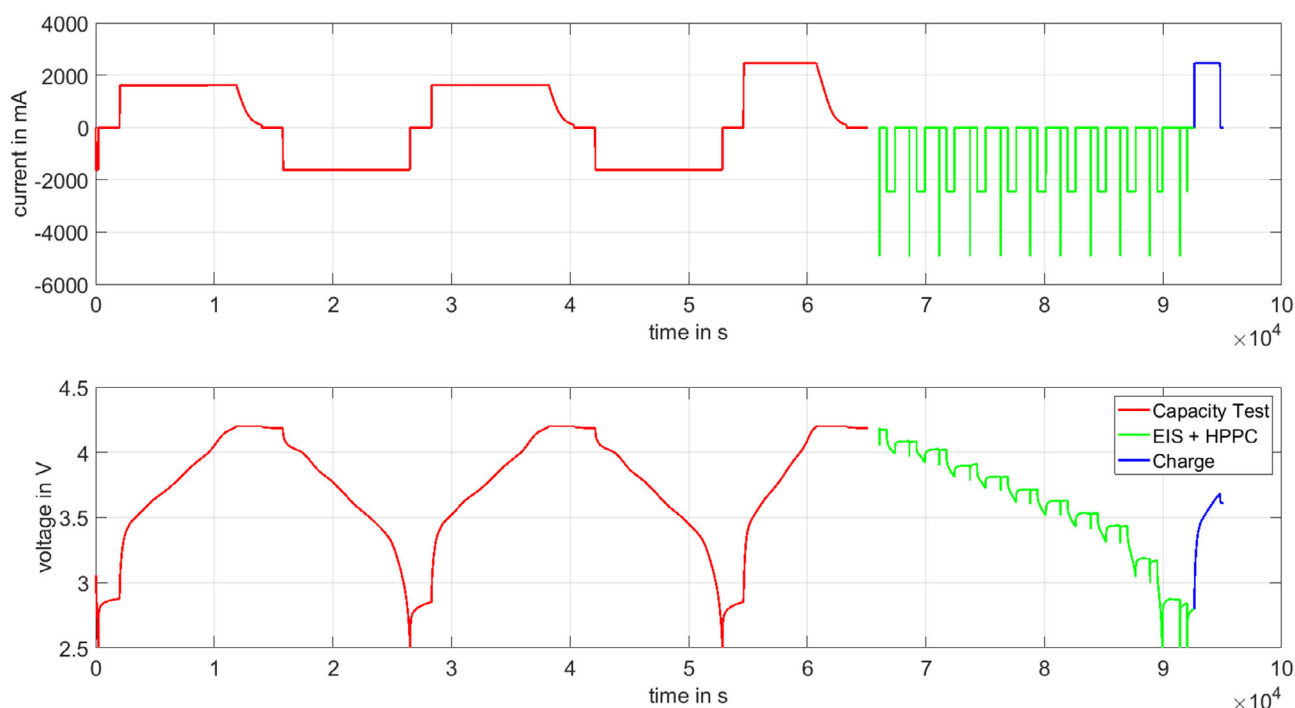


Figure 2. Current and voltage over time for C–R–Z test of NCA-HE cell with indication of capacity test, EIS and HPPC test and subsequent charge for next aging sequence.

different aging programs also might affect the aging, as the time spent under these conditions can either induce less or higher aging on the cells, compared to their aging program. The EIS test at SOC 0 and SOC 100 showed a different behavior than for the intermediate SOC's and as the wave of the sinusoidal signal or the reply could be outside the safety settings for voltage of the cell, it was sometimes not conducted perfectly or even stopped when those parameters were exceeded, leading to incomplete data.

2.6. Equivalent Circuit Fitting

To enable the extraction of information from impedance data, various kinds of equivalent circuit models (ECM) have been fitted to the impedance curves. This chapter provides an insight into the used equivalent circuit elements and the fitting procedure. Furthermore, a quick overview of the developed tool is given.

2.6.1. Background and Application

Various kinds of ECM can be used for the analysis of measured impedance data. These are classified by being physically motivated (PM-ECM) or electrically motivated (EM-ECM) models and differ in their description of the interfaces between individual components of the unit cell. **Figure 3** shows various kinds of equivalent circuit elements that are used to model the battery impedance. Not shown are standard elements as resistors, capacitors, and inductors. A parallel connection of a resistor and an inductivity (RL-element (a)) is used to model the high-frequency effects of the measurement setups inductive components on the resulting impedance spectrum.

This study utilizes PM-ECM because of their more exact representation of impedance behavior. Their main disadvantage is a missing Laplace-transformation for time-domain modeling, which

is not relevant for the undertaken analysis.^[15] EM-ECM describes ideal interfaces as a single process characterized by a single RC-circuit (Figure 3b) with the time constant $T = R \cdot C$. Due to the variation in particle sizes and inhomogeneous concentrations, realistic interfaces contain multiple processes with a distribution of time constants. In PM-ECM, this distribution is considered in the use of RQ-elements (Figure 3c). These elements use a deviation factor n to describe the spread of the summarized time constants. The impedance of such an RQ-element can be calculated as stated in Equation (1).^[8]

$$Z_{RQ}(f) = \frac{R}{1 + (j\omega T)^n} \quad (1)$$

Furthermore, two elements are used to describe low-frequency behavior of LIBs based on the Fick's laws of diffusion.^[9] The Finite-Length-Warburg element (FLW, Figure 3d) describes unrestricted diffusion of a species into the diffusion layer. Finite-Space-Warburg elements (FSW, Figure 3e) are being used, if the absorption capabilities for the diffusing species are limited. The corresponding equations are given in Equation (2) and (3).

$$Z_{FLW}(f) = R \cdot \frac{\tanh(\sqrt{j\omega T})}{\sqrt{j\omega T}} \quad (2)$$

$$Z_{FSW}(f) = R \cdot \frac{\coth(\sqrt{j\omega T})}{\sqrt{j\omega T}} \quad (3)$$

2.6.2. MATLAB Program Requirements

The SAFETY tool (StAte of hEalTh anAlYsis) has been developed on and is compatible with MATLAB version R2023b. For a successful launch of the program, the following toolboxes need to be

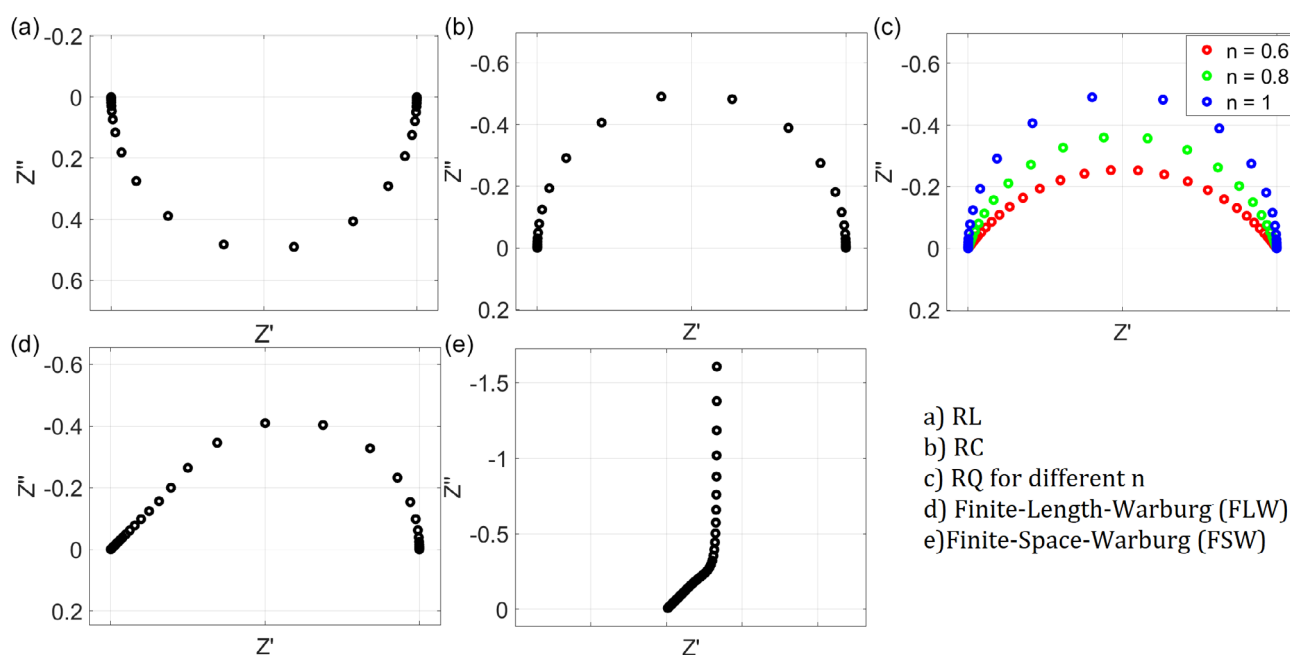


Figure 3. Nyquist plot of different impedance fitting elements: a) RL, b) RC, c) RQ, d) Finite-Length-Warburg, and e) Finite-Space-Warburg.

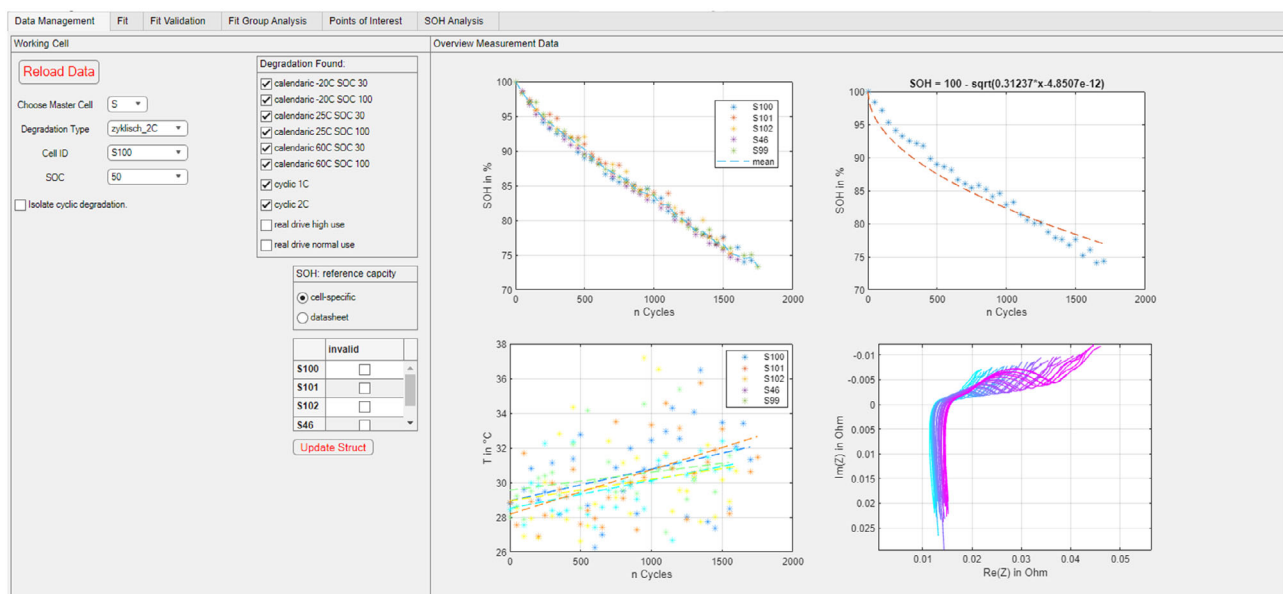


Figure 4. Screen caption of the SAFETY MATLAB program graphical user interface during impedance fitting process.

installed: curve fitting, data acquisition, optimization, state flow, and parallel computing.

2.6.3. MATLAB Program Design and Setup

For the analysis and processing of all measured data, the SAFETY-tool has been used. This tool covers all working steps from data management over impedance processing to the correlation of impedance parameters and SOH; a screen capture is provided in Figure 4.

Implemented functions for impedance processing cover fitting to PM-ECM and EM-ECM as well as points-of-interest detection based on the approach of Shabbir et al.^[11] To fit a set of impedance spectra, the user must first perform a reference fit on a single spectrum. Therefore, residuals from Nyquist and Bode representation are used as benchmark. The resulting set of parameters will then be used to process all provided impedance spectra, and results are stored in dimensions of SOC × T × SOH.

3. Results

3.1. Results for Useable Capacity

Cell aging was performed with the cyclers given in Table 2, and by the programs presented in Section 2.3, subsequently, the capacity was assessed as described in Section 2.4. Figure 5 shows the development of useable capacity for cyclic aging of all four battery types in dependence of transferred charge. As per definition, the end of life (EOL) is marked at 80% SOH. Values are mean values, and error bars are standard deviations, all obtained from the data of up to five different cells of same type and profile tested. As the values are mean values, the capacity value plotted, is not continuously decreasing. The plot of Cyc2 is scaled the same way

as Cyc1, but the axis is cut as SOH below 60% were not reached. The amount of transferred charge has been calculated from the number of load cycles using Equation (4).

$$Q = 2 \cdot n_{\text{cycles}} \cdot C_{\text{Battery}} \quad (4)$$

In the annex, the data is provided over equivalent full cycles in Figure S1, Supporting Information, and in Figure 5, it is plotted over transferred charge in kAh. Analyzing capacity loss with respect to transferred charge instead of number of equivalent full cycles (EFC) shows a significant difference in rate of degradation between the four cell types. The first set of cycles after the initial characterization results in a big step in capacity loss of ≈5–8% of cells NMC, NCA-HP, and LFP for both protocols. In comparison, cells of NCA-HE type do not show such a distinct step. The further course of degradation of NCA-HE cells shows a more comparable rate of capacity loss resulting in ≈12.5 kAh of transferred charge until reaching EOL for protocol Cyc1. The upward step in the middle of the NMC curve for Cyc1 can be explained by the stopping of aging of those cells with lower SOH because of their continuous overheating during cycling. Overall, the results of cells cycled with Cyc2 show a smaller variance in aging rates, as well as an unexpected slower aging of LFP cells compared to Cyc1. Aging with Cyc2 program showed a stable and comparable degradation behavior for most active materials until the end of study, except for NMC. However, with Cyc1 program, for the same transferred charge, the unstable degradation zone is reached, most significantly for NMC and LFP cathode material, resulting in fast capacity decrease and large scatter between the cells. Subsequently, the capacity degradation of the individual NMC and LFP cells for Cyc1 program is plotted in Figure 6 in a separate curve each, to gain a better understanding. The results for cycling with protocol Cyc1 show a wider variance in rate of degradation between identical cell models, especially for NMC and LFP cells. Because of this large variation, Figure 6 takes a closer look at each

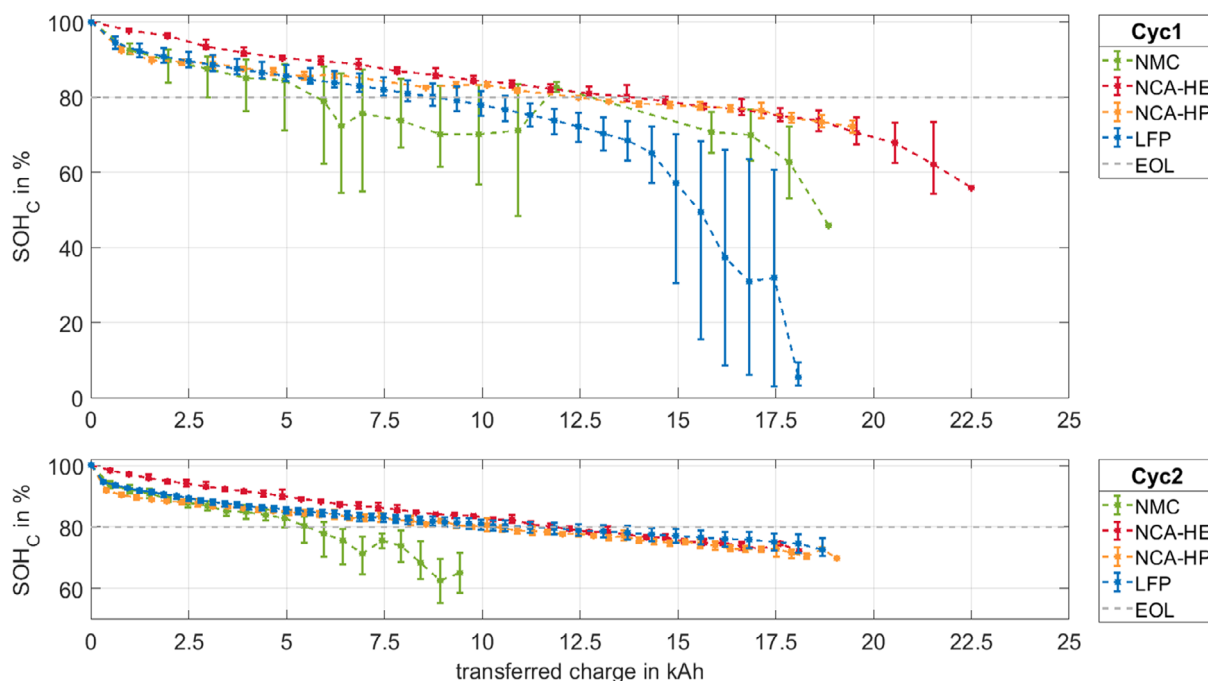


Figure 5. Mean SOH evolution over transferred charge, calculated with averaged capacity loss, during cyclic aging with profiles Cyc1 and Cyc2, shown are all four different cell types.

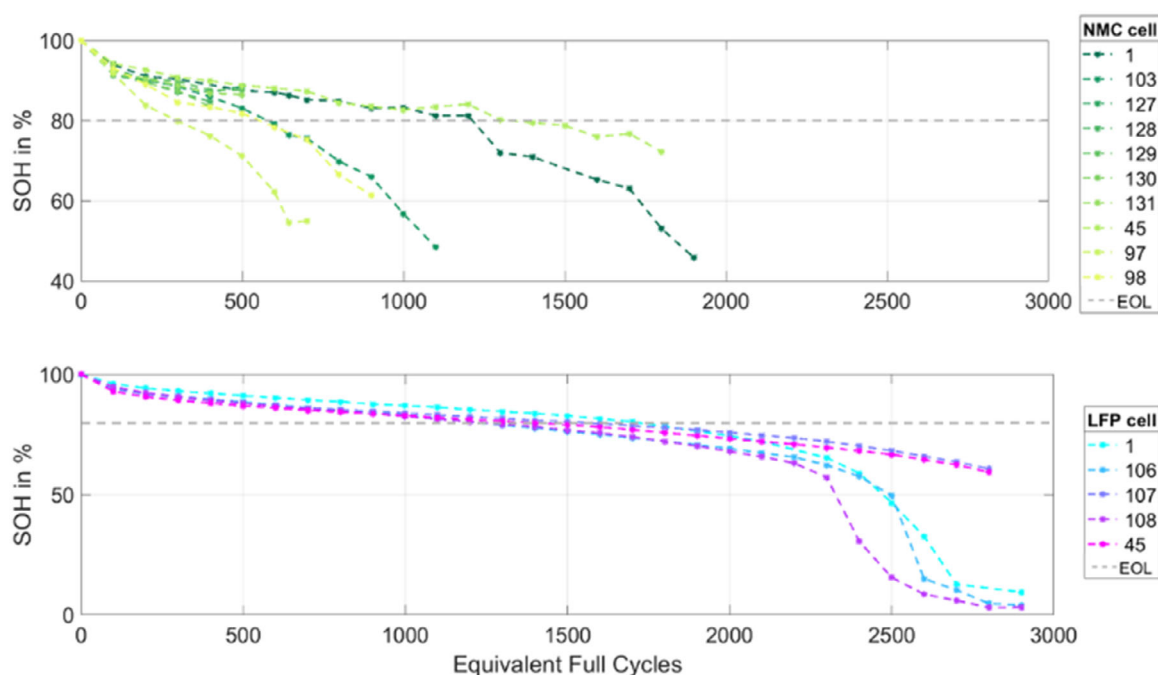


Figure 6. Individual SOH evolution, plotted for equivalent full cycles, during cyclic aging with profile Cyc1, shown are NMC (green) and LFP (blue) cells.

individual cell of these two battery types. The cyclic degradation through protocol Cyc1 leads to an inhomogeneous aging behavior for NMC cells; unstable rapid degradation is reached at different cycle numbers for the individual cells.

For further investigation, more cells of this type have later been added to this test, which results in more available data for low cycle numbers. LFP cells show less deviation for the first

2000 cycles of testing. Afterward, the SOH of three of the five cells starts falling dramatically, without earlier tendency to do so. Since there is no clear majority of similar aging behavior beyond 2300 cycles, no statement can be made which evolution beyond this mark can be expected and which is extraordinary.

The result of capacity fade by calendar aging is presented in **Figure 7**. Storing the cells at 60 °C leads to an accelerated

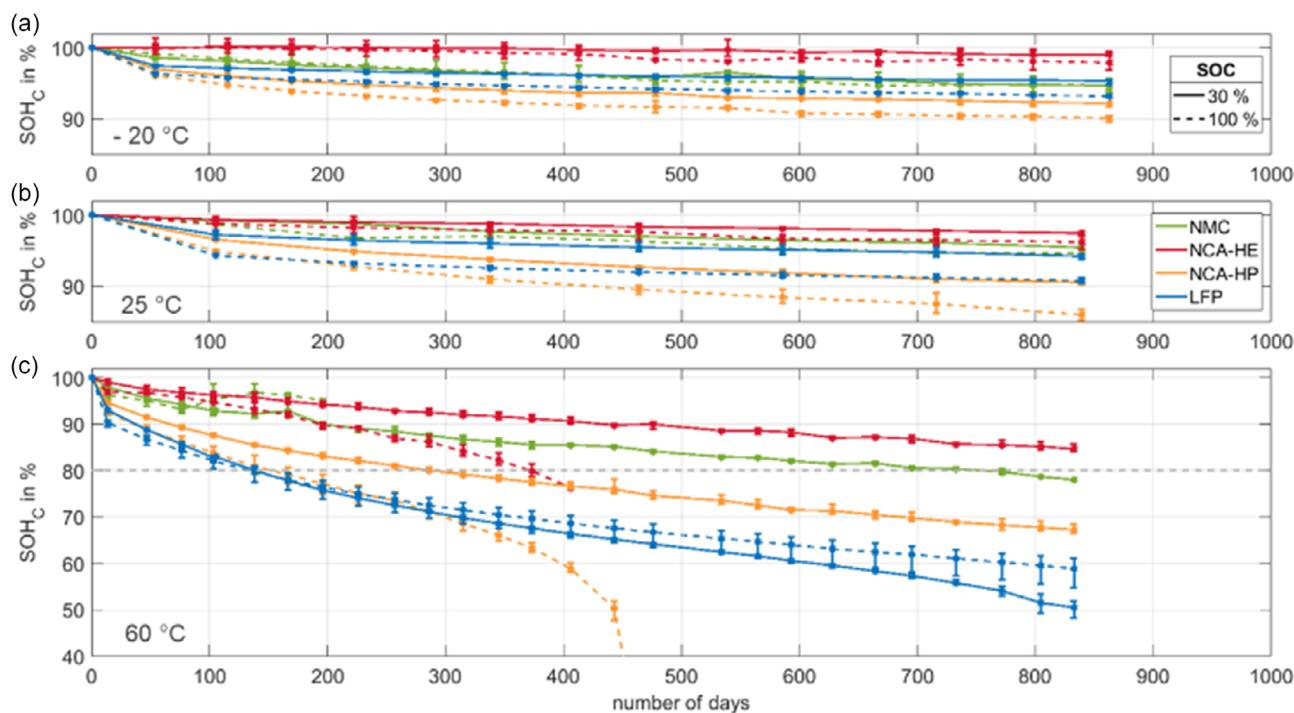


Figure 7. Mean SOH evolution over days of calendar aging, calculated with averaged capacity loss, for aging at SOC 30 and 100 at different temperatures, a) -20°C , b) 25°C , and c) 60°C , shown are all four different cell types. The SOC 100% NCA-HP curve in (c) is cut for scaling reasons, the last data point at 450 days for the SOH based on capacity is 7%.

decrease of capacity compared to the lower temperatures. This is consistent across all examined types of cell chemistry. The expected square root behavior of calendar aging can be assumed for all cells and temperatures with exception of NCA cathode cells at 60°C and 100% SOC. These cells show a sudden increase of degradation beyond 300 days, violating square-root-like aging behavior. With higher calendar storage temperature, an earlier capacity loss is observed for all cell types. As expected, most cells showed a faster aging for storing at high state of charge. Surprisingly, for calendar aging at 60°C , beyond a certain point, NMC and LFP cells stored at SOC 100 showed a slower degradation than cells stored at SOC 30. For NMC cells, this trend is explained by more cells at SOC 100 added later to the study, to get a better understanding; however, they all experienced the triggering of the current interrupt device (CID) because of inner pressure rise after less than 200 days of aging, most even at less than 100 days. For LFP, this trend is supported by more data and over a long time, as well as not disturbed by failure of cells, which therefore could show a different aging mechanism depending on high or low SOC storing regime.

3.2. Results for Qualitative Impedance Change in Nyquist Plot

To answer the question of interpretability of aging history from solely looking at impedance spectra of an aged cell, this section presents the impedance data for the four different cell types in Nyquist plots (real vs. imaginary part of the impedance signal). The effect on the impedance spectra due to cyclic degradation

is shown in **Figure 8**. For all cell chemistries, cyclic aging leads to an increase in Ohmic resistance. Furthermore, all cells but the ones with LFP cathodes experience a change in polarization resistance, leading to a rise of the diameter of the polarization semicircle. The clear development of local maxima and a change in shape of the polarization arch can be seen with progressed cell degradation of the NCA cells. The cyclic aging of LFP cells leads to a flattening of the polarization curve and a decrease of the polarization resistance. The influence of calendar aging on the shape of the impedance data is minimal for degradation at -20 and 25°C ; hence, it is not shown here. Instead, **Figure 9** shows the development through degradation for storage at 60°C with SOC 30 and SOC 100, where significant aging impact is found. All cells show a significant increase in Ohmic resistance as the useable capacity decreases. For NCA cells, the amount of Ohmic change shows a dependency of the storage SOC with an amplification at 100% SOC. Furthermore, all cells experience an increase of polarization resistance. This is especially distinctive for NCA cathodes, additionally showing the development of local maxima through a change of shape for the polarization semicircle.

3.3. Results for Ohmic Resistance from Impedance Test

The following subchapter shows the quantitative development of the Ohmic resistance by cyclic (**Figure 10**) and calendar (**Figure 11**) aging. The shown curves represent mean values of the impedance parameters of identical cells of an aging group. This kind of comparison has been judged valid due to a deviation of parameter values of 5% for Ohmic resistances and 10% for

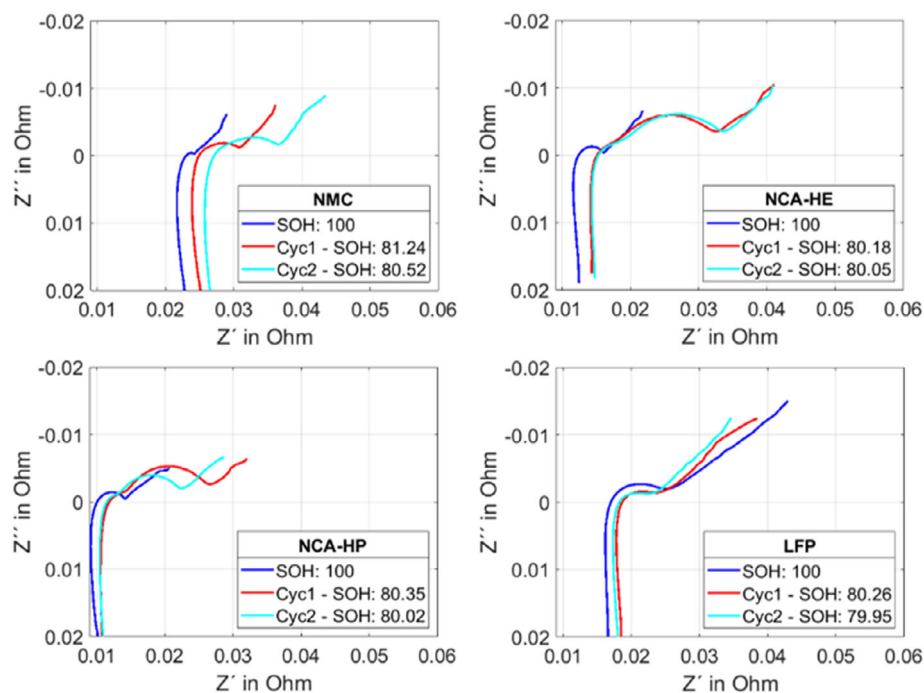


Figure 8. Nyquist plots of new state (blue) compared to states after cyclic aging with Cyc1 (red) and Cyc2 (cyan) protocol shown are all four different cells in separate graphs for each cell type. All Nyquist plots are captured at around 80% SOH.

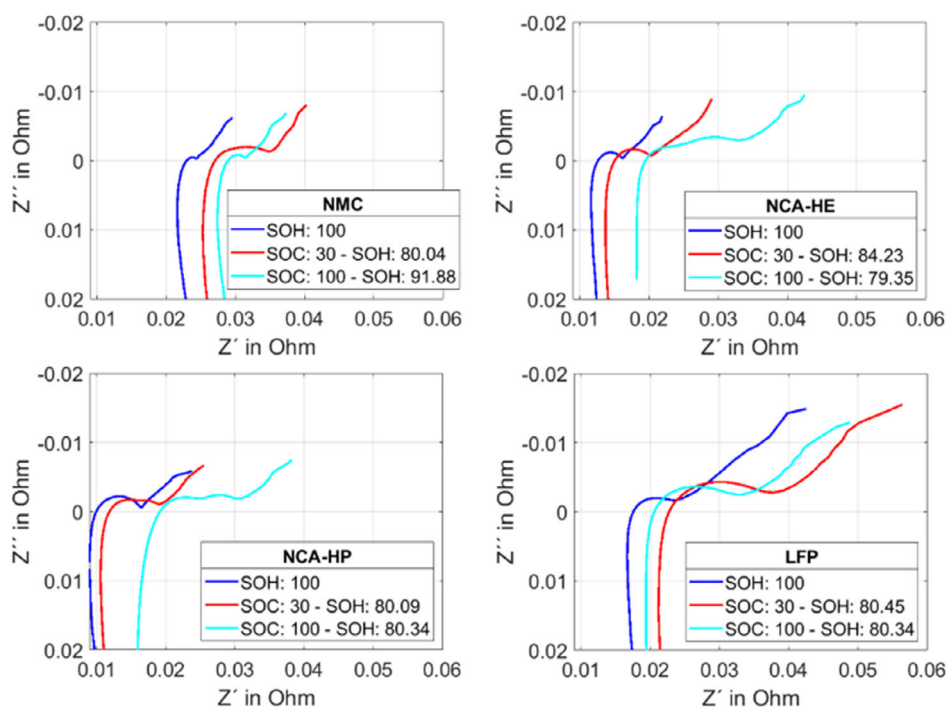


Figure 9. Nyquist plots of new state (blue) compared to states after calendar aging at 60 °C with SOC 30 (red) and 100 (cyan), respectively, shown are all four different cells in separate graphs for each cell type. All Nyquist plots are captured at around 80% SOH, except for the NMC cell stored at SOC 100%, as this SOH was not reached for this cell before failure after less than 30 days and could therefore not be captured.

polarization resistance. Both cyclic aging protocols in Figure 10 show an exponential growth of Ohmic resistance with decreasing SOH. Additionally, due to their faster loss in useable capacity over transferred charge, the cells with NCA and LFP cathodes show a

stronger increase of Ohmic resistance because of the lower load in protocol Cyc1.

The difference due to varying cell chemistries appears to be larger than the difference caused by the load parameters of the

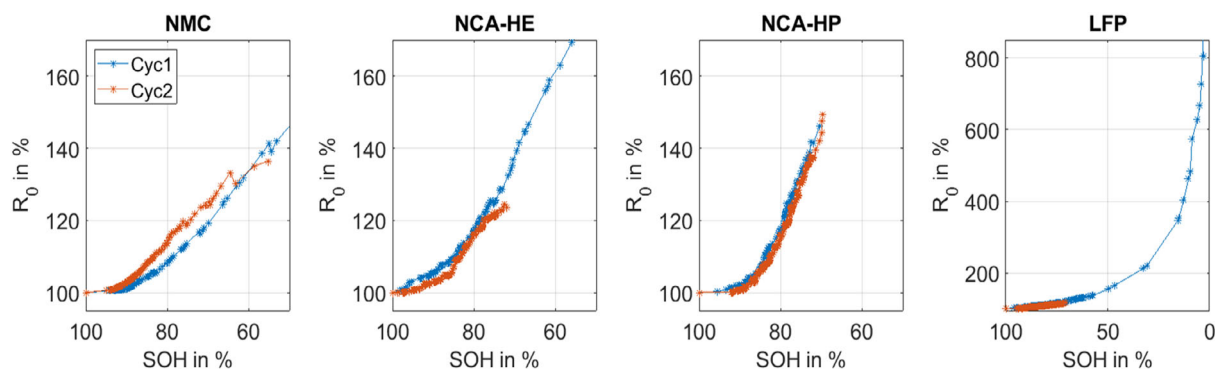


Figure 10. Mean Ohmic resistance growth during cyclic aging for Cyc1 and Cyc2 protocol, obtained from impedance test, shown for all four different cells in separate graphs for each cell type.

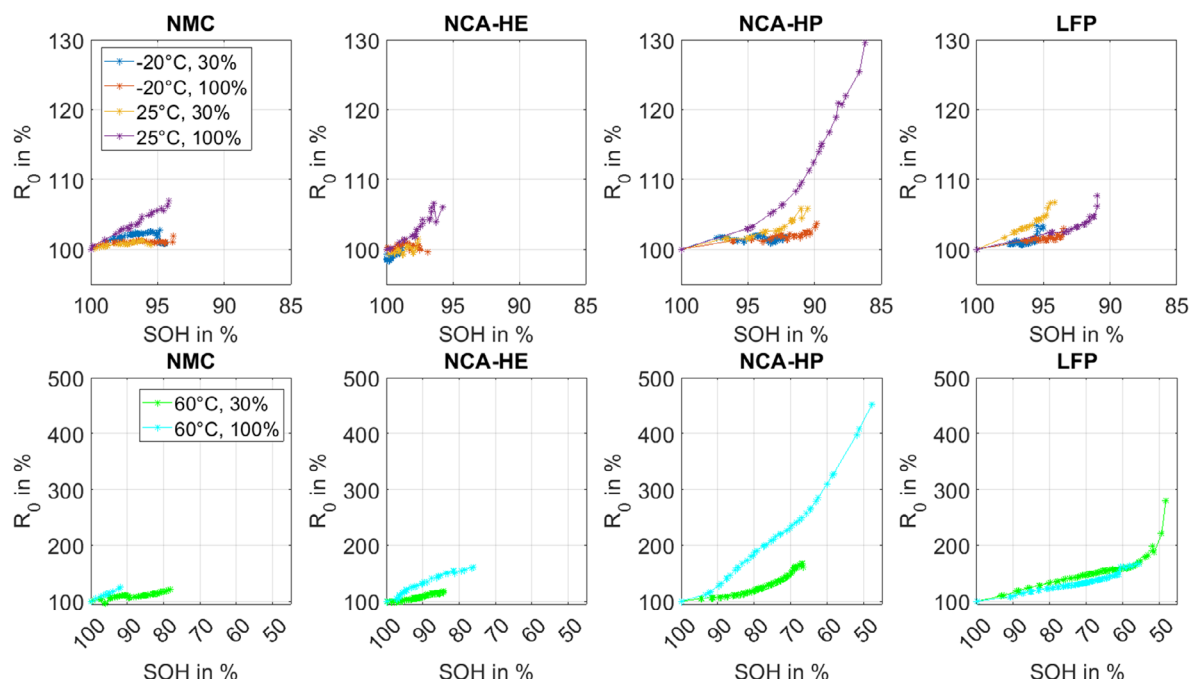


Figure 11. Mean Ohmic resistance growth during calendar aging at -20 and 25°C combined in one graph (top row) and 60°C (bottom row), each for cells with SOC 30 and SOC 100 respectively, obtained from impedance test, shown for all four different cells.

protocols. This becomes obvious when comparing the Ohmic increase of NCA cells to LFP cathode cells. After ≈ 1500 load cycles, EOL is reached by both NCA cells with a growth of $+20\%$ in comparison to $+10\%$ for LFP cells. Even though NMC cells show a moderate increase of resistance of $+10\%$ to $+15\%$ until reaching EOL, it must be considered that these cells reach EOL after ≈ 600 load cycles for both protocols. Hence, NMC cells experience the biggest increase of serial resistance per set of cycles, resulting in a gain of $+50\%$ in just 1000 cycles for protocol Cyc2. The particularly low SOH achieved by successfully cycling LFP cells with protocol Cyc1 close to 0% SOH clearly shows the approximate exponential behavior of the Ohmic resistance over the whole lifetime of the batteries. Even though these cells experience lower increase of Ohmic resistance until EOL than other cell chemistries, a massive increase of $+700\%$ toward 0% SOH must be considered for usage at sub-EOL levels of battery health.

As shown in Figure 11, calendar aging results in an Ohmic increase that is strongly dependent of both SOC and temperature at which the cells are stored. This increase is especially strong for higher temperatures. For NMC and both NCA cells, the combination of high storage temperatures and 100% SOC shows the biggest growth in Ohmic resistance. When compared to cyclic aging, it appears that calendar aging can result in a stronger growth of internal resistance until EOL. This depends strongly on the storage conditions and should be considered when evaluating the safety of an aged battery.

3.4. Results for Polarization Resistance

Following the investigation of the development of Ohmic resistance, the change in polarization resistance is shown for cyclic

(Figure 12) and calendar (Figure 13) aging. During the first few cycles, the polarization resistance of both NCA cells initially drops by $\approx 30\%$. Afterward, the process changes to approximate exponential growth. The development characteristic of the polarization resistance seems to be comparable between both cycling protocols. NMC directly starts with approximate exponential growth without the initial decrease. Until EOL, NMC, and NCA-HP cells gain around 200% in polarization resistance, while NCA-HE cells experience the biggest growth with plus 400%. A completely different characteristic is being shown by LFP cells with a decrease of 35% until EOL. For cell health levels below 50% SOH, LFP cells cycled with Cyc1, change their decrease of polarization resistance into a strong exponential gain, reaching nearly +2000% until SOH levels close to 0%. The development of polarization resistance due to calendar degradation process shows strong dependence of storage SOC and temperature. Different temperatures result in an altered direction of evolution meaning that polarization resistance can both increase and

decrease due to storage conditions. This is especially significant for cells with NCA cathodes. Both NCA cell types show strong declines in polarization resistance for temperatures below 0°C in opposition to exponential growth for storage at $+60^\circ\text{C}$. Only cells with NMC cathodes show a consistent direction of development for every used calendar aging protocol.

In the annex, a direct comparison of mean resistance and polarization resistance for the different aging conditions of cyclic aging is provided in Figure S2, Supporting Information, and for calendar aging for each temperature in Figure S3–S5, Supporting Information, respectively.

3.5. Results for Equivalent Circuits for NCA Cells

Following the extraction of PM-ECM parameters from impedance fits, SOH dependence of different partial resistances and time constants can be analyzed. Especially interesting elements are

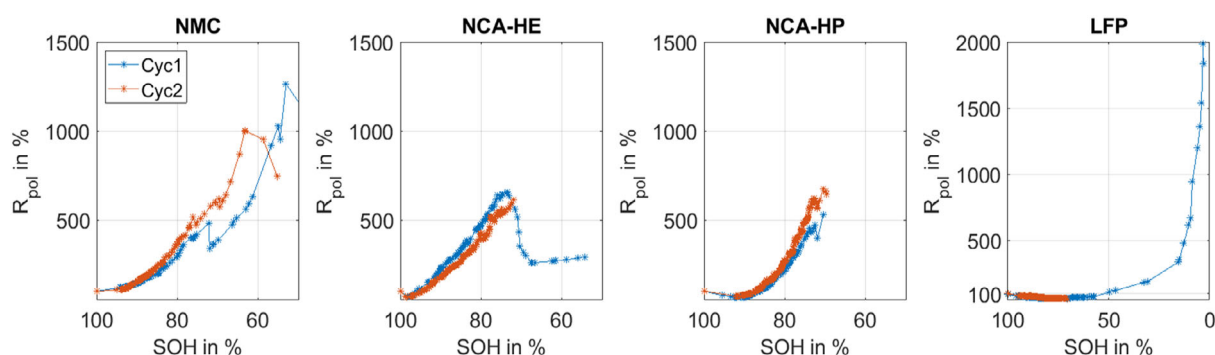


Figure 12. Mean polarization resistance growth during cyclic aging for Cyc1 and Cyc2 protocol, obtained from impedance test, shown for all four different cells in separate graphs for each cell type.

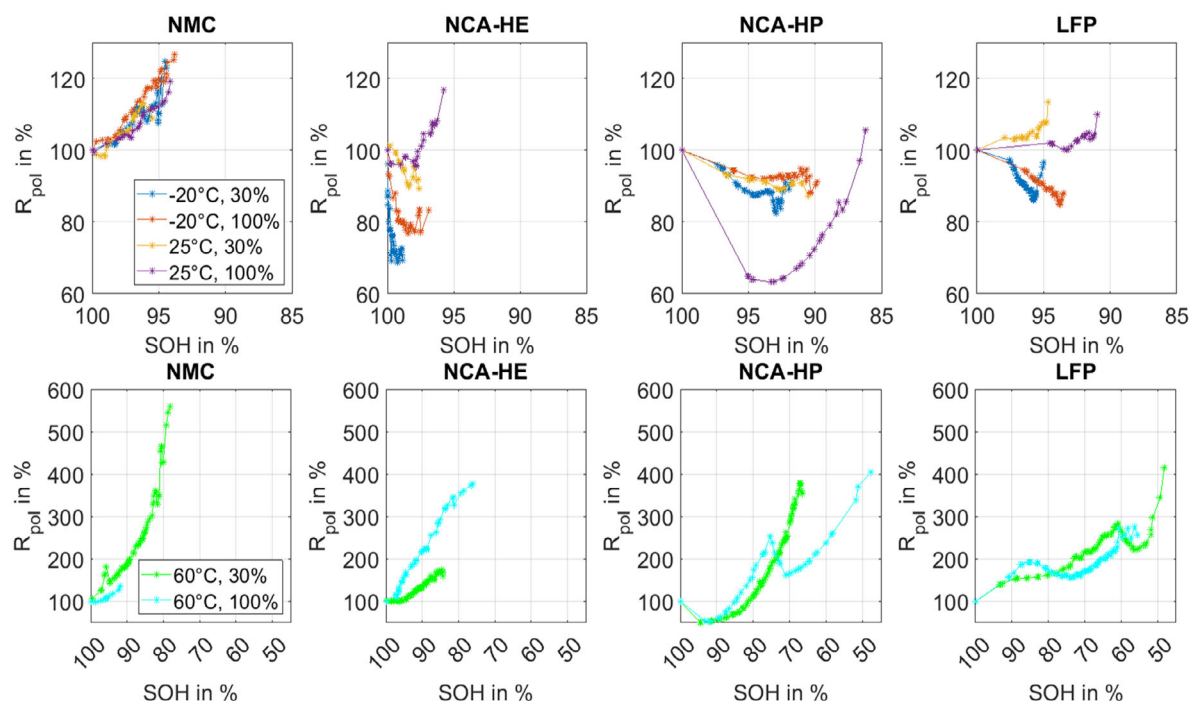


Figure 13. Mean polarization resistance growth during calendar aging at -20 and 25°C combined in one graph (top row) and 60°C (bottom row), each for cells with SOC 30 and SOC 100 respectively, obtained from impedance test, shown for all four different cells.

the serial resistance—linked to contact degradation and electrolyte decomposition—and parameters of the polarization resistance, linked to degradation of interfaces and electrode decomposition. The used ECM for NCA cells degraded by cyclic aging consists mainly of a serial resistance (Ohmic resistance), two RQ elements (polarization resistance), and an FLW element (diffusion). Additionally, a parallel RL-element and a capacitor have been used to account for inductive and capacitive influences of the measurement setup. As can be seen in **Figure 14**, for the NCA-HE cell, the partial resistances and their SOC-relation show a strong dependence of SOH.

Ohmic resistance R and partial polarization resistance $RRQ2$ show the beforehand mentioned exponential increase due to progress in degradation. Especially with $RRQ2$, the typical U-shape of this parameters SOC dependency gets more pronounced for lower SOH. While $RRQ1$ direction of development is not as clear, as for the other elements, a slight loss with SOH can be interpreted, even though the total impedance of the battery is growing. In comparison to the other two elements, the relative change of this parameter's resistance is small.

Furthermore, the fitted ECM parameters have been used to evaluate the ratio of single polarization elements to the total

polarization resistance following the idea of Kallel et al.^[7] To describe the correlation of SOH and parameter ratio, we used a hyperbolic tangent function as shown in Equation (5) instead of a linear approach as proposed by Kallel et al.

$$P_{\text{ratio}} = A - B \cdot \tanh(C \cdot (100 - \text{SOH}) + D) \quad (5)$$

Figure 15 on the left shows the mean course of parameter ratio of $RRQ1$ or $RRQ2$ to R_{pol} over SOH-level for NCA-HE cells cycled with Cyc2. This course has been fitted to Equation (5) containing parameters A to D to describe the relationship between the chosen parameter ratio and the SOH. Afterward, the inverse of the fitted equation has been used to validate the described relationship by inserting the parameter ratio values of a single cell and determine the corresponding SOH level. Therefore, **Figure 15** on the right compares the SOH as extracted from capacity measurements ("from capacity") to the SOH as extracted from the ratio of a partial resistance $RRQ1$ to R_{pol} ("from resistance").

For observation limited by BOL and EOL, an exponential approach might seem suitable, but the chosen window of observation points toward tanh-functions to deliver a better description. In comparison to the linear approach by Kallel et al.^[7] the tanh-function achieve a more exact characterization below 95% SOH. The link between SOH and parameter ratio

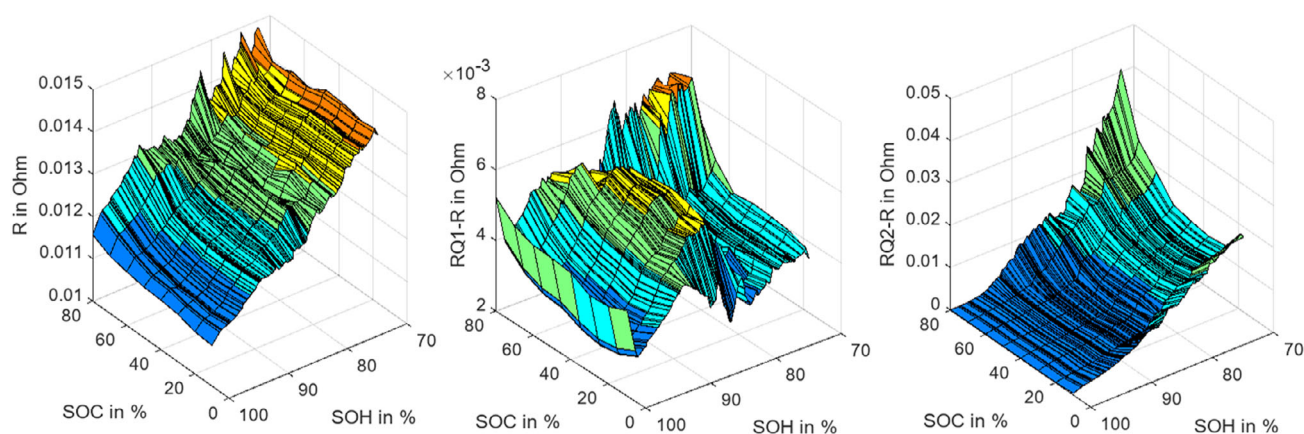


Figure 14. Evolution of Ohmic resistance R and polarization resistances $RQ1$ and $RQ2$ from NCA-HE cell from cycling aging with Cyc2 Protocol in a 3D representation with SOC and SOH represented in space.

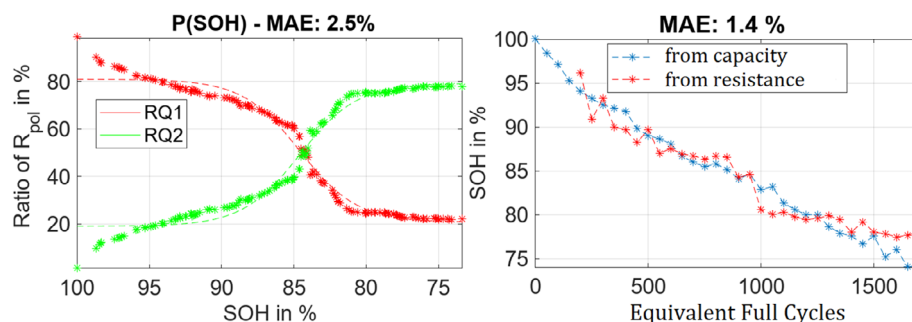


Figure 15. Polarization resistance ratio for $RQ1$ and $RQ2$ for different SOH (left) and SOH over equivalent full cycles compared between derived from capacity and from resistance components of EIS measurement (right).

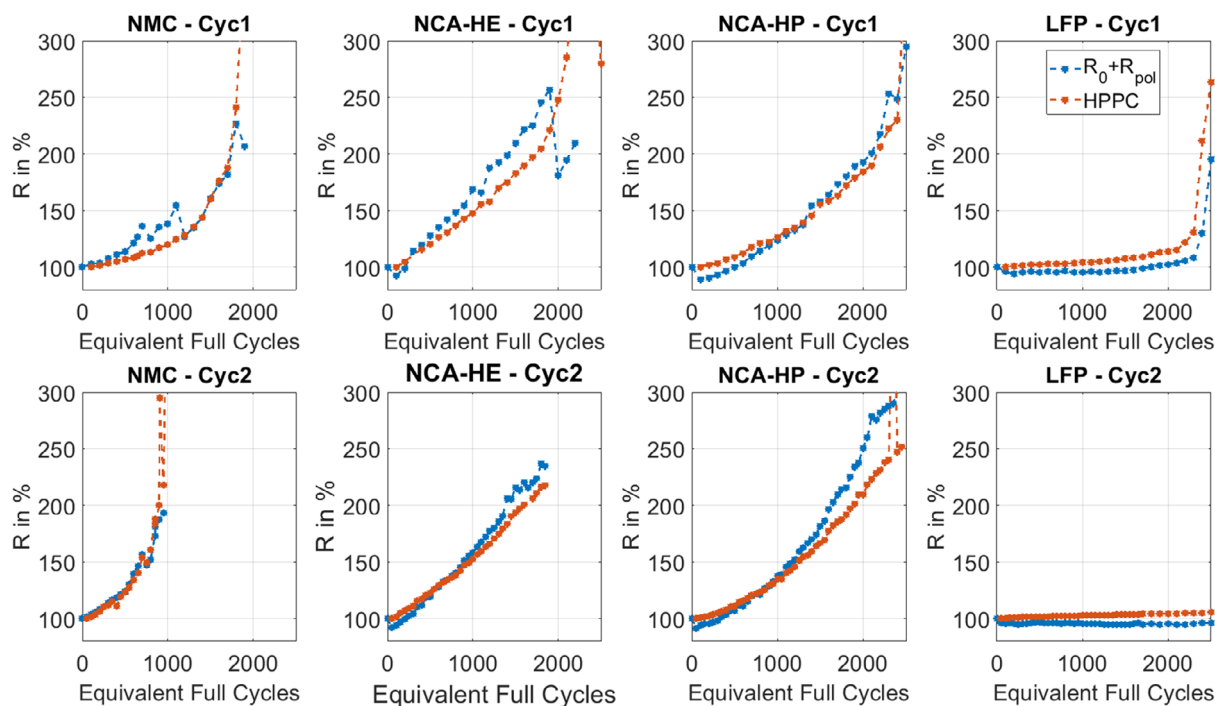


Figure 16. Comparison of serial resistance calculation from EIS spectrum (blue) to HPPC (red) for cycling aging protocol Cyc1 and Cyc2, shown for all four different active materials.

by tanh-function delivers the best results for high gradients of parameter ratio over SOH (in the region between 90 and 80% SOH) but lacks precision for lower gradients below EOL. This kind of description lacks the ability to describe the relationship in quasi-static regions of the s -function.

3.6. Comparison of Ohmic Resistance from Pulse Discharge (HPPC) Compared to those Obtained from EIS Spectra

Besides logging capacity and impedance data, HPPC tests have been performed along the aging studies. As shown in **Figure 16**, the relative change of pulse resistance has been compared to the relative change of $R_0 + R_{pol}$ from the impedance spectra as recommended for this kind of comparison by Saha et al.^[16] In general, the two curves show a comparable behavior. Especially for NMC cells, the curves of HPPC and EIS parameters match very well. A significant difference can be observed over the course of degradation for LFP cells and in the beginning for both NCA-HE and NCA-HP cells. Based on an initial loss of polarization resistance, the sum of R_0 and R_{pol} decreases when compared to the manufacturers state of the cell. Especially for LFP cells, a constant offset between EIS resistance values and HPPC resistance can be seen. Considering the much larger effect of voltage hysteresis for LFP and NCA compared to NMC, the observed offsets between HPPC and EIS parameters for the different cell chemistries have been suspected to be strongly allocated to hysteresis effects. This assumption is being strengthened through a study by Ovejas et al.^[12] dealing with the effect of aging on the voltage hysteresis of LFP cells.

4. Discussion

4.1. Performance of the Different Cathode Materials

4.1.1. NMC Cells

Most significant for the behavior of cells with NMC cathode material in this study is their larger scatter of data between individual cells for the same aging conditions, compared to other cells studied in this work. The most evident case occurs for cyclic aging, especially cells aged with Cyc1 program. Additionally, these cells show the earliest failure of all cells for most aging conditions. Cell failure is defined either by the cell being not chargeable anymore, for example, because of CID triggering, or when maximum temperature is repeatedly reached during cyclic aging. End of life or SOH 80% of NMC cells for cyclic aging protocols is reached after 5 kAh of transferred charge; systematic cell failure before 10 kAh of transferred charge is reached; however, some cells sustained the aging better and were usable nearly twice as long.

In general, for calendar aging, NMC cells aged faster than NCA-HE cells, but slower than NCA-HP and LFP cells, for most conditions examined. With a closer look, at -20°C , NMC performance is very close to LFP cells. At 25°C their performance is even like NCA-HE cells, with the slowest aging at this condition. At 60°C , the cells stored at SOC 100% failed the earliest of all cells and in a larger scatter, always in 200 and most in less than 100 days, while other cathodes sustained at least 400 days storage with SOC 100% at 60°C . Cells that were charged to 30% SOC sustained the 60°C calendar aging with a faster capacity fade than NCA-HE, but slower than NCA-HP and LFP cells.

EIS spectra analysis at SOH 80% showed a larger impact on the real part of the impedance spectrum of NMC cells for cyclic aging, and the impact of the different discharge rates between Cyc1 and Cyc2 at the same SOH was more severe than for other cathode materials. Moreover, the shape of the impedance spectrum remained similar after the aging for the NMC cathode, mainly for cycling aging but mostly also for calendar aging at 60 °C. This aging path led to a more severe impact on the full Nyquist plot of the NMC cells, compared to NCA-HE cells, but less severe than NCA-HP.

The derived Ohmic resistance from EIS shows the largest difference between Cyc1 and Cyc2 for the NMC cell. The trend of the polarization resistance for the NMC cell is different to all other cells. Between resistance derived from EIS and resistance obtained by HPPC for cyclic aging, the NMC cell shows for Cyc1 a significant difference for some of the data points and a good accordance for others. Cyc2 only shows a difference for the two methods at the end of life of the cells. Mean Ohmic resistance from calendar aging shows a faster resistance growth over the SOH compared to NCA-HE, but a comparable behavior compared to both type NCA cells. Only a small growth in resistance is found for calendar aging at 60 °C before the end of life of the cell. From the mean polarization resistance, the calendar aging for NMC cells shows a very comparable and parabolic resistance growth for all aging conditions, besides the much more severe absolute growth of SOC 100% at 60 °C. This is unique for NMC; the other cathodes show a distinct effect of each temperature and SOC for storage on the shape and growth rate of mean polarization resistance.

We conclude for NMC cells a more severe aging under certain conditions that can be captured by several analysis techniques and different aging mechanism than NCA cells, but a close overall degradation under our test conditions.

In the annex in Figure S6, Supporting Information, for the NMC cathode material, the impact of cyclic aging, both on capacity loss, as well as on resistance growth, is directly compared over equivalent full cycles.

4.1.2. NCA-HE Cells

In general, the NCA data in this paper is supported both by the NCA-HE cell and NCA-HP cell performance that we describe, which mostly varies only slightly in terms of aging, proving the reproducibility of the data we collected and the validity of the observations for the individual active materials.

Taking a closer look at the NCA-HE cell, for both cycling with Cyc1 and Cyc2 program, this is the only cell that does not show a rapid capacity loss at the beginning of cycling and has a better performance in terms of capacity over most of the cycling and until reaching SOH of 80%. After this threshold, NCA-HE and NCA-HP cells perform identically. Only for Cyc2 program, the LFP cells shows a better aging behavior beyond SOH 80% than the NCA cells.

Additionally, in calendar aging at –20, 25, and 60 °C, NCA-HE cells have the best aging behavior for storage with SOC 30% of all compared cathode materials with the lowest capacity loss of all.

Only storage with SOC 100% at 60 °C shows a faster aging than any SOC of the other active materials, and at this condition, it is only aging faster than NMC at SOC 30%. But, after reaching SOH 80%, these cells fail soon when stored with SOC 100 and at 60 °C, later than NMC cells, but earlier than LFP and NCA-HP cells at SOC 100 and all cells at SOC 30%.

The Nyquist plot for cyclic aged NCA-HE cells is subjected to severe shape change from aging, but nearly identical from Cyc1 and Cyc2 at 80% SOH, which is very distinct for this cell, and only one other cell, LFP, shows similar resemblance for different aging conditions at same SOH. NCA-HE shows the largest impact on the imaginary part of all active materials that we compared. Calendar aging at 60 °C influences the Nyquist plot by a comparable real part, to the other cells, and a visible impact on imaginary part for the cell stored at SOC 100%, resulting in a shape change, which is comparable to the impact for NCA-HP cell at the same storage SOC.

The mean Ohmic resistance from impedance measurement grows higher for Cyc1 aging than for Cyc2, the reached value before end of life, for NCA-HE is the highest after LFP. For calendar aging, the growth is less severe for NCA-HE cells until end of life, than for the other cells. The polarization resistance data from calendar aging at 60 °C grows very fast, especially for storage at SOC 100%. It shows an interesting behavior for Cyc1 aging: First, Cyc1 generates a faster growth of this resistance than Cyc2, and second, beyond SOH 80%, a sudden resistance drop is observed, followed by a very slow growth. As for LFP cells, the different calendar aging conditions are very distinct on their individual impact on polarization resistance growth for the NCA-HE cell, which is not as clear for the other cells. As for NCA-HP cells, the polarization resistance is shrinking for some aging parameters, such as storage at –20 °C. Serial resistance derived from EIS and HPPC for NCA-HE have mostly the same trend but are different absolute values for most of the data points, for Cyc1, the difference between the methods is the most severe, especially toward high degradation.

To summarize the NCA-HE cell behavior, while the aging behavior is under multiple conditions less severe than for NMC, it does not reach as low states of health before cell failure than NCA-HP and LFP cells. This cell type has unique behavior that can be observed, for example, in the resistance growth derived from EIS at certain levels of aging and for certain conditions. Each diagnostic method we used revealed different information about the ongoing aging of the NCA-HE cell.

Figure S7, Supporting Information, in the annex compares the overall aging of the NCA-HE cell from cycling and provides an overview.

4.1.3. NCA-HP Cells

During cyclic aging, NCA-HP cells perform similar as NMC and LFP cells, during the stable phase of aging. They keep a linear capacity decline for a long time, even after SOH 80%, and when the decline is not linear anymore, it still shows the slowest decrease of all cells. As NCA-HE cells, they perform as good and age as stable as those cells beyond SOH 80%, which is the best

performance of all cells for Cyc2 and nearly as good as LFP cells do at Cyc2 aging.

Furthermore, calendar aging behavior of NCA-HP cells is faster than of most other cells. While these cells perform worst for aging at -20°C and for SOC 100 at 25°C , they show a capacity loss for NCA-HP cells stored at SOC 100%, as LFP cells do with SOC 30% at 25°C , and for a long time, the same observation can be made for SOC 100% at 60°C . While the NCA-HP cells stored at SOC 30% at 60°C age slower than LFP cells, the cells stored at SOC 100 age, as mentioned above, similar until about 300 days of storage and then start to rapidly decline in their capacity.

In the Nyquist plot, cyclic aged NCA-HP cells show similar development of real part until EOL while comparing the influence of Cyc1 and Cyc2. In contrast to NCA-HE cells, the resulting imaginary part differs significantly. Interestingly, Cyc1 shows a more severe modification of the imaginary part of the Nyquist plot for NCA-HP than Cyc2 does. Moreover, for calendar aging at 60°C , NCA-HP cells show a similar behavior as NCA-HE cells do, such as a clear change of both real and imaginary part for storage state of charge 100% than for 30%, which is not observed for NMC or LFP.

The Ohmic resistance deduced from EIS reaches comparable absolute values as NMC for cyclic aging with a similar growth rate as NCA-HE showed and very close between Cyc1 and Cyc2. Moreover, calendar aging Ohmic resistance growth is growing to the highest measured values of all cells, for 60°C and SOC 100% at 25°C . Especially for 100% SOC for 25 and 60°C , a more linear than parabolic and rapid mean Ohmic resistance growth is observed. The polarization resistance is comparable for most parts of cyclic aging data and like NCA-HE, at the beginning with a resistance drop and then to NMC, where Cyc2 is more severe than Cyc1. However, the polarization resistance data from calendar aging of this cell is unique: Especially SOC 100% at 25°C shows a very severe resistance decrease at the beginning of aging, and SOC 100% at 60°C has a discontinuity in the curve, where a resistance decrease after SOH 80% is followed by another growth after SOH 70%. As for NCA-HE, about the comparison of impedance test and pulse discharge for resistance measurement of cyclic aged cells, both have the same trend for NCA-HP but have different values in most individual points of testing.

Thus, we can state that the NCA-HE and NCA-HP cells, which share the same cathode material, but different cell constructions, such as current collector thickness or numbers of internal tabs, show different aging behavior and different responses to the diagnostic approaches while following an overall common trend. This effect might be due to the different electrolyte composition that is used from the two manufacturers of HE and HP cell.

The NCA-HP cyclic aging is summarized by Figure S8, Supporting Information, which can be found in the annex.

4.1.4. LFP Cells

This cathode chemistry is known for a very good cyclic stability, and our data from Cyc2 protocol is proving this, where LFP shows the best aging behavior, not only for equivalent full cycles, but also for transferred charge, where the smaller capacity of this cell

is considered for the calculation. Unexpectedly, for Cyc1 protocol, LFP cells aged faster than other cells beyond a certain SOH and showed a faster decline in capacity than for Cyc2 protocol, with higher discharge current. We also noted a large scatter, and a detailed look at the individual data of the cells for Cyc1 in Figure 4 showed that two out of five cells had a stable and mostly linear capacity decline until nearly 3000 cycles; however, the three other cells of same type, batch and with the same cycling protocol, lost rapidly their capacity beyond 2200 cycles with 1 C discharge and were aged to a very low SOH of only 0.02% in one case in a very short time and while still functioning well. For calendar aging, LFP cells aged faster than NCA-HE and most NMC cells. The best performance of LFP is found at -20°C , where they behave as NMC cells; at 25°C their performance is a bit better than NCA-HP but at 60°C , they show the fastest loss of capacity of all cells, however while staying operational. Here, LFP cells at SOC 100% have a positively outstanding performance, compared to all other cells, as they were still functional after aging more than 800 days at 60°C fully charged, while no other cell tested sustained more than 450 days.

EIS analysis and graphical representation in Nyquist plots show a different imaginary component for the LFP cell, which is expected. Cyc1 and Cyc2 aging only have a small impact on the Nyquist plot, with a little more severe impact on real and imaginary part for Cyc1 than for Cyc2. While for cyclic aging until SOH 80% the LFP cells show the overall smallest change of the Nyquist plot of all cells for calendar aging, the inverse is seen for calendar aging at 60°C , as a very distinct shift is observed, which is strongest for state of charge 30% instead of 100%, and therefore much different to the other cathode compositions.

The EIS derived Ohmic and polarization resistance for Cyc1 program, with a very low SOH reached, is several times higher for the LFP cell than for the other cells. This data provided here is unique and goes down to nearly a SOH of 0%, as the cell was still working, despite the extreme aging. All resistance growth from cyclic aging is smaller for LFP over a large interval of the SOH, especially the mean polarization resistance only grows beyond a SOH of 50%. Calendar aging results show a similar trend for the mean Ohmic resistance as for the other cells; however at 25°C , a faster degradation is observed than for NMC and NCA-HE. Very low SOH can be reached from storage at 60°C for the LFP cell, with no cell failure and mostly linear mean Ohmic resistance growth, though the polarization resistance at 60°C cannot be described with a single law and is marked by several increases and decreases over the aging. At a temperature of -20°C , polarization resistance shows a decrease; at a temperature of 25°C , an increase is observed for both SOC. There is a general offset between the resistance from EIS and from HPPC test, as well as a small resistance loss at the beginning, which goes below 100%, that can only be found in EIS data; HPPC always stays above 100%. Overall, both still show the same trend for LFP cells from cyclic aging.

LFP cells show in summary, a different impact of cycling rates and storage state of charge on the aging severity than for the other cells, resulting in a more difficult estimation of the aging. Very low states of health were reached in our study, as the cells remained operational despite the very severe degradation.

In the annex, we provide in Figure S9, Supporting Information, a summary of the cyclic aging of the LFP cell, for both capacity and resistance.

4.2. Severance of the Different Aging Routes

4.2.1. Cyclic Aging Subheading

Two different cycling aging profiles Cyc1 (1 C discharge) and Cyc2 (2 C discharge) were used for the experiments in this study; a higher C-rate would not have been allowed for all the cells in the comparison and would have exceeded operating temperature of some cells even in the new state.

The cycling took place over more than 2 years, and very low SOH values were reached by some cells. For each cell type and cycling program, at least five individual cells have been tested with the same program and during the same time. Consequently, we can evaluate the impact of the aging on each cathode active material, as well as the scatter between the aging performance of the different cells of the same active material.

We found that for the SOH, calculated based on the cell capacity, the aging between Cyc1 and Cyc2 is overall similar. While most cells reach SOH 80 at about 12.5 kWh of transferred charge for Cyc1, they already do so at 10 kWh for Cyc2 program. Moreover, stable (or linear) capacity decrease ends at about 15 kWh of transferred charge for most cells with Cyc1 aging. However, Cyc1 showed a much larger scatter than Cyc2 cycling, and a problematically large scatter was observed for NMC cells for both programs and for LFP cells for Cyc1 program. Because of this large scatter, the aging behavior we observed in this zone of SOH cannot be directly attributed to the performance of the active materials, as it could be due to individual cell failure or due to different aging mechanisms. Fortunately, the large scatter only occurs below SOH of 80%, clearly indicating the difficulty of studies beyond this SOH and the novelty of this data.

Subsequently, an interesting observation for the capacity loss can be made, as NCA-HE and most significantly LFP cells show an earlier capacity loss for same transferred charge for Cyc1 program, than for Cyc2 program, with a higher discharge current. As the cells are charged both with 0.5 C and CC-CV conditions, most aging effects should come from the discharge phase and apparently a more reversible discharge program leads to a faster aging, than fast irreversible discharge. Furthermore, the increase of serial resistance for Cyc1 program is faster over the SOH.

From the Nyquist plot, a similar impedance spectrum for the cells aged with Cyc1 and Cyc2 program was found for the NCA-HE cell, but not for the other cells. Cyc2 program with 2 C discharge led to a more distinct change of the spectrum for NMC cell, but not for the NCA-HP and mostly the LFP cell, where a higher modification results from Cyc1 program.

For cyclic aging, analysis of the mean Ohmic resistance from the impedance spectrum is a good way to track aging and allows for extrapolation for most cells and might be extrapolated over large ranges of SOH, for LFP down to 50% SOH, where the slope of growth finally increases. Compared over the SOH, only for NMC cells Cyc2 lead to a faster growth of the mean Ohmic resistance

for the same SOH than for the other cathode materials until about SOH 60%, where it is reversed. The polarization resistance from the same EIS analysis is not possible to be extrapolated to track aging and has much more differences between the cells and numerous changes. The end of the linear aging of NCA-HE cells in Cyc1 around an SOH of 70% can very clearly be observed in the sudden drop of polarization resistance at the same SOH. For all cells, except NCA-HE, Cyc2 aging leads to a faster growth of polarization for the same SOH than Cyc1.

Resistance values calculated from EIS spectra compared to those derived from HPPC pulse discharging are, as discussed in detail for each active material, not the same and are showing different slopes, but similar trends for Cyc1 and Cyc2 as well as for the different cells, except beyond 2000 cycles, where no clear trend can be derived. While HPPC data allows for extrapolation to forecast further aging, the Ohmic resistance from EIS test shows much larger variation in the individual points and can only be extrapolated for the LFP cell.

As mentioned in the sections before, in Figure S6–S9, Supporting Information, that can be found in the annex, the cyclic aging effects on capacity loss and resistance growth plots are summarized for each cathode material in one diagram.

4.2.2. Calendar Aging

When the cell aging performance between the different storage temperatures is compared, it is slowest for -20°C , as expected, followed by 25°C and far more severe at 60°C . It should be noted however that storage at 25°C for about 2 years leads to a SOH of below 90% for the NCA-HP cell stored with SOC 100%.

Interestingly, storage at SOC 100% compared to SOC 30% showed some cases, where it is not more severe for cell aging, but exceptionally even leads to slower capacity loss at some phases during the aging process. This is the case for 60°C for the NMC cells, but only for the cells, that sustained more than 100 days of storage without triggering of the CID, because of rising gas pressure inside the cells. Additionally, LFP cells beyond SOH 70%, aged at 60°C , performed better when stored at SOC 100% than 30%, in the form of a slower capacity loss, reaching about 5% higher SOH at the end of the test.

Nyquist plots from calendar aging are only shown for 60°C , because of the little aging effect of -20 and 25°C . While storage at SOC 100% resulted in a bigger modification of the impedance spectrum for all cells, it was smaller for LFP cells, compared to SOC 30%. Moreover, at comparable SOH of 80%, NCA-HE and NCA-HP cells stored at SOC 100% showed a several times higher real part of the Nyquist plot and additionally significant modification of the imaginary part.

Mean Ohmic resistance analysis for calendar aging shows a different growth rate for each aging condition and cell, which are parabolic for some combinations, and subjected to more changes in the growth rate over the aging but might still be used for extrapolation to estimate following degradation. A higher SOC for storage has different impact on the aging, for LFP cells at all temperatures SOC 30% lead to a faster Ohmic resistance growth, similar for NMC cells at -20°C , but different to all other cells,

temperatures, and SOC. The polarization resistance is, as for cyclic aging data, not possible to be extrapolated and shows high variation for all four cell types, and no clear trend can be found. Cyc1 leads to faster growth than Cyc2 for NCA-HE as mentioned, and SOC 30 at 60 °C does the same for NMC cells and for some intervals of SOH below 80% also for NCA-HP and LFP cells. A very strange polarization resistance behavior is found for NCA-HP cells aged at 25 °C with SOC 100%, and very similar growth for –20 °C as for 25 °C and with both SOC is observed for NMC cells.

In summary, for calendar aging, capacity loss and Nyquist plots, are the only reliable and comparable ways to track and forecast further aging.

4.3. Capabilities of the Diagnostic Techniques Employed

4.3.1. Capacity Testing

Capacity testing does not need any complicated or costly equipment and can be done in the device that cycles the cells. Nonetheless, this test takes more time than several pulse discharge tests or EIS spectra measurements. This is due to the fact that the capacity test should be done with a low C-rate, and to exclude irreversibility effects from operations with higher C-rate than the test C-rate, two full cycles at this rate should be performed, to get a precise value of the cell capacity. Of course, if a less precise value is sufficient, capacity test can be performed much faster or even included in normal operations. In this investigation, capacity data was a good metric to track the aging, and, by looking at the behavior over time, stable or unstable aging could be identified. However, the SOH evolution in Figure 7 for calendar aging at 60 °C shows a nearly identical behavior of capacity loss for LFP cells as for NCA-HP cells at SOC 100%, but suddenly, beyond 300 days, the curves start to evolve much differently, NCA-HP in a rapid aging, the other, continuously in a linear decrease. This behavior could not have been predicted based on capacity measurement and trend analysis. Moreover, Figure 6 showed a very rapid degradation for some of the cells beyond 2300 cycles, while others with the same aging program and cycle count are still in a linear zone of capacity loss.

4.3.2. EIS Spectra

To perform impedance analysis, specific test devices are needed, and some understanding of the cell and test apparatus performance is required to set the correct measurement conditions. Further, understanding and availability of electrochemical models is required to perform fitting of the test data. Of course, this higher complexity gives a lot of more options for prediction models, adaption to specific use conditions and defining of application tailored test programs. EIS testing will always be the most expensive and complex way to get an understanding over the progression of aging but is far from being too difficult for real world applications and should be considered in industry to enable best use of expensive batteries built with limited availability raw materials.

An obvious disadvantage of EIS that has been shown by our results is that a clear classification of aging history as a distinction between different calendar or cyclic utilization patterns simply through qualitative analysis of the shape of an impedance spectrum is not possible. Even though the qualitative analysis of impedance spectra allows no claims about the cells strain history, quantitative methods proved to be suitable to analyze the cells current state of aging through its impedance parameters. A clear correlation between the development of Ohmic and polarization resistance values and aging progression has been validated by the found results. This correlation has been confirmed to progress below the usual SOH limit of EOL. The extensive difference in magnitude and direction of change in impedance parameters between different cell chemistries and aging profiles points toward EIS being an important tool for estimating an aged cells safety regarding second life usage besides the usual evaluation through remaining cell capacity.

Furthermore, parameters extracted from EIS fitting have shown to allow a comparison of partial resistance values of the polarization resistance to the overall development of polarization resistance. This makes EIS a suitable tool to pre-identify the magnitude of aging of certain parts of a battery and assess the further focus of examination on cell components in more elaborate and destructive test methods.

While the mean Ohmic resistance allows for extrapolation to forecast further degradation during aging, polarization resistance curves were found to have numerous irregularities occurring during the aging and therefore should not be extrapolated for this purpose. Nevertheless, in Figure 12 for NCA-HE under Cyc1 aging, the following fast decrease in capacity beyond SOH of 70% can be clearly predicted from the drastic polarization resistance drop.

As mentioned previously, in the annex, a direct comparison of the mean and polarization resistance obtained from EIS testing is given in Figure S2, Supporting Information, for both cyclic aging protocols and in Figure S3, S4, and S5, Supporting Information, for each temperature and both storage state of charges.

4.3.3. Pulse Discharge (HPPC) Testing

This test is very simple and fast, but must be carried out with caution, especially at low SOC to prevent operation of the cell below allowed conditions or to reduce the risk associated with cell overheating from fast discharge.

The comparison of HPPC and EIS data for cyclic aging has pointed toward HPPC appearing to be able to show aging effects on the hysteresis of batteries, especially for LFP, that do not show in data from impedance spectra. Since hysteresis seems to have a big influence on the voltage–current relation of aging LFP cells, HPPC leads to valuable—and in terms of cell safety important—information that cannot be extracted from the more complex method of impedance spectroscopy.

An extrapolation of HPPC data seems to be suitable for large ranges of the SOH to predict further cell aging.

Altogether, this method is a very promising tool for aging analysis and forecast.

4.4. Comparison of Aging Behavior to Literature

An aging study by Preger et al.^[1] on type 18 650 LIB cells with NMC, NCA and LFP cathode material is conducted. We aim to compare our results to this study, as well as to provide a comparison from 18,650 to 21,700 cells in this section. The loss of initial capacity over equivalent full cycles for cyclic aging with C-rates of 0.5, 1, and 2 C observed by Preger et al.^[1] shows the slowest capacity loss for LFP cells of up to 4000 cycles to reach 80% capacity loss, followed by NMC with more than 2000 cycles and lastly NCA with up to 1600 cycles. We found in our study for C-rates of 1 and 2 C a more severe aging behavior and faster capacity loss, probably because of the higher C-rates. The considerably slower aging of LFP cells was also observed in our study; however, the NMC cells studied in our experiments aged noticeable faster than the NCA cells, both NCA-HE and HP, which is a different observation than Preger et al.^[1] made. Three phases of degradation, initial sudden drop because of lithium consumption for SEI formation, followed by linear degradation from lithium side reaction-controlled loss and a rapidly occurring, final capacity loss at cell failure from impedance increase are observed in our capacity loss data, in accordance with literature, for cyclic and calendar aging. Some of the NMC cell data shows a less stable second phase, with higher variation in capacity loss, which is due to earlier single cell failure, affecting the mean value. For calendar aging at -20 and 25 °C, terminal rapid capacity loss is not observed, as our cells did not fail during the nearly 900 days of storage at those temperatures. For 60 °C, only the cells stored at SOC 100% showed failure and left the phase of linear capacity loss.

The detailed comparison of capacity loss between Preger et al.^[1] for cycling aging at 1 and 2 C, from 0 to 100% SOC, for the different cathode materials to the corresponding data of our study, reveals a similar reach of SOH 80% for NMC cells with Cyc1 and 1 C cycling, after 600 cycles. Additionally, a similar scatter between the different cells is observed, and 2 C cycling of some cells of Preger corresponds well to our averaged capacity loss data. We observed a longer lifetime for NCA cells, with 1400 cycles for Cyc1 on NCA-HE, compared to around 450 cycles for 1 C in Preger et al.^[1] and 1200 cycles for Cyc2 on NCA-HE, to nearly 600 cycles for 2 C.

However, we observed a lower lifetime of LFP cells, reaching SOH 80% after 1300 cycles for Cyc1, and Preger found more than 2000 cycles for a capacity loss of only 5% with 1 C cycling. Both our study and Preger observed for some cells with more severe aging conditions a slower capacity degradation than for others with a less severe aging, which confirms a general scatter from cell to cell for identical aging conditions that must be considered for systems design with commercial cells.

We are therefore confident that the behavior of our cells is confirmed by Preger et al.^[1] and that we can extend the knowledge for SOH below 80% and to type 21,700 cells with our study.

In Waldmann et al.^[17] the dominating aging mechanism is estimated based on the calculation of $\ln(r)$ with the aging rate r and a temperature dependent component, based on an Arrhenius function. Comparable data for an NMC-LMO cell of Waldmann et al.^[17] and for commercial cylindrical NMC and

LFP cells from Preger et al.^[1] is represented in a graph of $\ln(r)$ over the temperature, as cycling was performed at different temperatures in those papers. Moreover, this graph allows to extract a value for comparison at 20 °C, where we performed our cyclic aging test. We found that the calculated value for $\ln(r)$ for our NCA-HE cells, both for Cyc1 and Cyc2, is nearly identical to the value of the curve of $\ln(r)$ values for NMC of Preger et al.^[1] that has a negative slope, which is indicating a lithium plating dominated aging mechanism. The values for NCA-HP are also very close to the NMC curve of the literature and surprisingly the value for our LFP cells as well. This is corresponding to a significant difference to the LFP curve of Preger et al.^[1] which equals an $\ln(r)$ of -6 for cycling at 20 °C, while we found -3.1 for Cyc1 and -3.3 for Cyc2. It is therefore not possible to conclude whether our LFP cells also have SEI growth as dominating aging mechanism under these operational conditions. Our $\ln(r)$ value for NMC is with -2.1 for Cyc1 and -2.2 for Cyc2 higher than Preger et al.^[1] with $\ln(r)$ of -3 for NMC. However, it is therefore in between the data for NMC of Preger et al.^[1] and for NMC-LMO of Waldmann et al.^[17] which both indicate lithium plating as dominating aging mechanism. In Preger et al.^[1] this dominating mechanism is found for all NMC aging data, while Waldmann et al.^[17] found it only until 25 °C.

5. Conclusion

Our aging study allowed us to compare four different cathode materials with a similar graphite anode (only the anode of the LFP cell is without silicon). The fastest degradation, both for calendar aging and cyclic aging, was found for NMC cells.

The NCA-HE cells have a different cell design than the NCA-HP cells, to achieve their different strengths, being high energy for longer travel distance in EV applications or high power for fast acceleration. We found the aging between the cell designs to be different and especially that other degradation information is revealed, depending on the methods we used to track the aging. However, for most parameters, a similar trend and still a smaller difference than compared to other cell chemistries, such as NMC or LFP, is observed. Under most conditions, the slowest degradation was found for NCA-HE cells. While LFP cells were only aging slower in comparison to the other cells under Cyc2 aging, they remained operational for very low SOH close to 0 from Cyc1 aging. Therefore, this study provides unique data for low SOH, especially for LFP cells.

We provided data for degradation from two modes of aging, cyclic, and calendar aging with different parameters (C-rates, temperatures, and SOC of storage) for type 21,700 cells, the severity of each method is different for the cathode compositions and cell designs, as compared and presented. It is notable how the state of charge of storage for calendar aging leads to cell failure in less than 200 days compared to over 800 days, for the same NMC cathode material. While cyclic aging could be tracked and estimated based on mean Ohmic resistance derived from EIS test, the latter is much more diverse and difficult for calendar aging.

By employing three diagnostic approaches and regular testing of the cells during aging, a large database for capacity loss, resistance growth, and impedance change was established and presented. It was found that the same aging has a different impact on the data from the diagnostic approaches, and some effects are only captured by some methods. Also, depending on the cathode materials, the diagnostics can reveal different behaviors.

In our study, capacity loss is in several cases a good method to assess the progression of the aging of a cell; however, it is not always the best way and comes with limitations. Some rapid cell degradations, such as the one of the NMC cell stored with SOC 100% at 60 °C, are not detected before the end of life, by triggering of the CID from gas formation inside the cell, from any of the diagnostic approaches we use.

While the Nyquist plot is subjected to numerous possible impacts from aging, which are different for cathode materials and aging parameters, the deduced resistance growth for Ohmic resistance from the EIS data shows clear aging indications and allows to track cell aging with precision, though we observed this resistance growth to be neither strictly linear or parabolic and neither to be explained by a single law or distinct phases, especially for the polarization resistance component. It can be concluded that while resistance data from impedance comes with more information than capacity loss, it is harder to be fitted, extrapolated, and interpreted. The HPPC analysis can be implemented into production and systems much more easily and cheaper than EIS analysis; in our comparison of their resistance growth values from the two methods, we found an offset for some cells and aging conditions, as well as very good accordance for others. Different zones of high mismatch between the methods, while still staying both valid to track the aging, are observed, though still showing different cell behavior during degradation and sometimes a large offset at the end of life, though some aging effects were only detected by HPPC and not by the much more complex EIS testing. Considering the very deep states of health we reached in our study, this shows the limitations of both methods for states of health below 80% and for rapid cell aging processes to estimate further aging.

An aging study of this size for type 21,700 cells has not been reported previously and our findings underline that the existing knowledge for other cylindrical cells can be transferred to type 21,700 cells as well.

Moreover, the cells from this aging study are either opened after aging and a subsequent material scientific analysis of the active material with different techniques is done, or they are tested for their thermal abuse safety in heat–wait–seek tests with accelerating rate calorimetry. The results of both investigations will be reported in the future, compared to new cell safety behavior from ref. [14]. Those reports will be especially interesting, because of the low SOH reached and the entirety of the analysis of aging, materials condition, and cell safety.

Acknowledgements

The authors acknowledge funding from Helmholtz Association in the program Materials and Technologies for the Energy Transition (MTET). This work contributes to the research performed at CELEST (Center of Electrochemical Energy Storage Ulm-Karlsruhe). The authors would like to thank for the help of Philipp Finster, Claire Floras, and Sophia Heinzmann for this aging study, by supporting lab work or data treatment.

Open Access funding enabled and organized by Projekt DEAL.

Conflict of Interest

The authors declare no conflict of interest.

Data Availability Statement

The data that support the findings of this study are available from the corresponding author upon reasonable request.

Keywords: aging · capacity · electrochemical impedance spectroscopy · lithium-ion battery · ohmic resistance

- [1] Y. Preger, H. M. Barkholtz, A. Presque, D. L. Campbell, B. W. Juba, J. Román-Kustas, S. R. Ferreira, B. Chalamala, *J. Electrochem. Soc.* **2020**, *167*, 120532.
- [2] S. Abada, M. Petit, A. Lecocq, G. Marlair, V. Sauvart-Moynot, F. Huet, *J. Power Sources* **2018**, *399*, 264.
- [3] P. Teichert, G. G. Eshetu, H. Jahnke, E. Figgemeier, *Batteries* **2020**, *6*, 8.
- [4] P. Kuntz, O. Raccurt, P. Azais, K. Richter, T. Waldmann, M. Wohlfahrt-Mehrens, M. Bardet, A. Buzlukov, S. Genies, *Batteries* **2021**, *7*, 48.
- [5] Y. Preger, L. Torres-Castro, T. Rauhala, J. Jeevarajan, *J. Electrochem. Soc.* **2022**, *169*, 030507.
- [6] X. Feng, D. Ren, S. Zhang, X. He, L. Wang, M. Ouyang, *Int. J. Electrochem. Sci.* **2019**, *14*, 44.
- [7] A. Y. Kallel, V. Petrychenko, O. Kanoun, *Appl. Sci.* **2022**, *12*, 885.
- [8] S. Gantenbein, *PhD Thesis*, Karlsruher Institut für Technologie (KIT) **2019**.
- [9] J. N. Illig, *Dissertation*, Karlsruher Institut für Technologie **2014**.
- [10] R. Wagner, D. Lowenstein, in *2007 IEEE Autotestcon*, IEEE, Baltimore, MD **2007**, pp. 1–5.
- [11] H. Shabbir, W. Dunford, T. Shoa, in *2017 IEEE Transportation Electrification Conf. and Expo (ITEC)*, IEEE, Chicago, IL **2017**, pp. 108–112.
- [12] V. J. Ovejas, A. Cuadras, *Sci. Rep.* **2019**, *9*, 14875.
- [13] A. Kalk, M. C. Holocher, S. Ohneseit, C. Kupper, M. Hiller, in *2023 IEEE Int. Transportation Electrification Conf. (ITEC-India)*, IEEE, Chennai, India **2023**, pp. 1–6.
- [14] S. Ohneseit, P. Finster, C. Floras, N. Lubenau, N. Uhlmann, H. J. Seifert, C. Ziebert, *Batteries* **2023**, *9*, 237.
- [15] D. Andre, M. Meiler, K. Steiner, C. Wimmer, T. Soczka-Guthund, D. U. Sauer, *J. Power Sources*, **2011**, *12*, 5334.
- [16] B. Saha, S. Poll, K. Goebel, J. Christophersen, *IEEE Autotestcon*, Baltimore, MD **2007**, pp. 646–653.
- [17] T. Waldmann, M. Wilka, M. Kasper, M. Fleischhammer, M. Wohlfahrt-Mehrens, *J. Power Sources* **2014**, *262*, 129.

Manuscript received: November 9, 2024

Revised manuscript received: March 14, 2025

Version of record online: